Numerical study on seasonal variations of gaseous pollutants and particulate matters in Hong Kong and Pearl River Delta Region

Roger H. F. Kwok,[1,2] Jimmy C. H. Fung,[1,2] Alexis K. H. Lau,[2] and Joshua S. Fu[3]

Received 13 July 2009; revised 1 March 2010; accepted 23 March 2010; published 24 August 2010.

[1] This study presents Community Multiscale Air Quality (CMAQ) model results for Hong Kong (HK) and the Pearl River Delta region in January, April, July, and October 2004, representing winter, spring, summer, and autumn seasons. Two sets of observations/measurement data are referred to in order to evaluate model performance. The first set consists of hourly observations of criteria pollutants at HK Environmental Protection Department (HKEPD) ambient stations throughout HK, while the second set contains speciated PM measurements, sampled at 6-day intervals, at six of the HKEPD ambient stations. Model-observation agreement is good in PM species sulfate, organic carbon (OC), and elemental carbon (EC). The good performance for OC and EC, when compared to similar evaluation for North America and Europe, demonstrates the importance of correct speciation in an emission sector. Underprediction of NOx and NH_3 suggests a desperate need of emission estimation improvement in these species. PM levels are higher in autumn and winter, lower in spring, and lowest in summer, coinciding with northeasterly winds due to continental outflow in autumn and winter, and with southwesterly monsoon in summer. The model is also able to reproduce the seasonal and spatial patterns for PM and O_3. In terms of PM composition, the model agrees with the measured fractions of sulfate, OC, and EC. Additionally, CMAQ was rerun with emission sources partially removed, with results suggesting that pollution sources beyond the Pearl River Delta also contribute to the PM and sulfate levels in HK, particularly during the winter season.

Citation: Kwok, R. H. F., J. C. H. Fung, A. K. H. Lau, and J. S. Fu (2010), Numerical study on seasonal variations of gaseous pollutants and particulate matters in Hong Kong and Pearl River Delta Region, *J. Geophys. Res.*, *115*, D16308, doi:10.1029/2009JD012809.

1. Introduction

[2] Like many other Asian cities, Hong Kong (HK) has been experiencing air pollution problems [*Chan and Yao*, 2008], visibility impairment being an indicator of ambient particulate matter (PM) levels. In Hong Kong, PM problems are contributed to both by local sources such as roadside vehicles [*Tsang et al.*, 2008], and by sources outside the territory. In fact, the increasing frequency of low visibility days from late 1990s up to 2003, in parallel with increasing Pearl River Delta (PRD) emission upwind of HK [*Wang*, 2003], suggests the regional contribution to ambient PM levels. *So et al.* [2007] found that there has been a 36% increase in ambient sulfate ($SO_4^=$) levels from 2000–2001 to 2004–2005. Since the beginning of this century, many researchers have concentrated their efforts to understand PM in Hong Kong [*Fang et al.*, 1999; *Ho et al.*, 2002, 2003; *Yu et al.*, 2004; *Cheung et al.*, 2005; *Chow et al.*, 2005; *Louie et al.*, 2005a; *Wai and Tanner*, 2005; *Ho et al.*, 2006; *X. F. Huang et al.*, 2006; *So et al.*, 2007] and in the neighboring Pearl River Delta (PRD) region [*Cao et al.*, 2003a, 2003b; *Wu et al.*, 2003; *Duan et al.*, 2007], with most focusing on the analysis of measured and observed data.

[3] In general, diverse research groups have arrived at the following conclusions. First, the chemical composition of ambient PM in Hong Kong is spatially uniform, in particular sulfate ($SO_4^=$), organic carbon (OC), and elemental carbon (EC), which accounts for about 30%, 40%, and 10% of $PM_{2.5}$ mass, respectively. Second, continental outflows import sulfate [*Ho et al.*, 2002, 2003; *Cheung et al.*, 2005; *Louie et al.*, 2005b; *Wai and Tanner*, 2005; *So et al.*, 2007; *Guo et al.*, 2009] and OC [*Ho et al.*, 2002; *Cao et al.*, 2003b; *Ho et al.*, 2003] into Hong Kong. *Cheung et al.* [2005] deduced that, on the basis of temporal variation of PM composition with changing synoptic wind flows, regional outflows from the PRD inland and coastal cities contribute ~48%–57% of $PM_{2.5}$, ~66%–72% of OC, and ~18%–20% of sulfate. Studies based on satellite Aerosol Optical Depth (AOD) [e.g., *He et al.*, 2008] also suggest regional transport of PM into the territory. For adequate air quality management in

[1]Department of Mathematics, Hong Kong University of Science and Technology, Kowloon, Hong Kong.
[2]Division of Environment, Hong Kong University of Science and Technology, Kowloon, Hong Kong.
[3]Department of Civil & Environmental Engineering, University of Tennessee, Knoxville, Tennessee, USA.

0148-0227/10/2009JD012809

Hong Kong, it is necessary to develop models that capture these key features in the observed data so that models can be used with confidence to develop emission control strategies and policies on transboundary pollutant transport.

[4] Currently there are two major approaches in air quality modeling: observation-based and emission-based. In addition to simple statistical analysis of observations and measurements, the observation-based approach also includes more sophisticated statistical models. To date, HK/PRD PM studies have employed principal component analysis (PCA) [*Wu*, 2003; *Ho et al.*, 2006; *Guo et al.*, 2009], cluster analysis [*Ho et al.*, 2006], unmix/positive matrix factorization [*Yuan et al.*, 2006], and chemical mass balance (CMB) [*Zheng et al.*, 2006] approaches. These techniques primarily aim at identifying emission sources, assuming that PM species in each source are known.

[5] Emission-based models are numerical ones. They require simulated meteorological inputs and emission data to be estimated beforehand. The models are run on the basis of implemented physical and/or chemical processes. No a priori knowledge about observations is required, and hence the performance can be assessed on the basis of the difference between the simulations and the observations.

[6] To date, numerical models have been applied to HK/PRD to study both photochemical species [*Streets et al.*, 2006; *J. P. Huang et al.*, 2006; *Wei et al.*, 2007] and PM [*Streets et al.*, 2006; *Feng et al.*, 2007]. *Streets et al.* [2006] focused on the impact on PRD air quality by industrial sectors using the global model STEM-2K1. The use of this model, however, perhaps meant spatial resolution was compromised. While *J. P. Huang et al.* [2006] classified ozone episodes into different underlying weather conditions, *Wei et al.* [2007] estimated the impact of biogenic VOC on ozone levels during a tropical cyclone event. A separate PM study by *Feng et al.* [2007] was also temporally confined to another tropical cyclone event. In all of the numerical studies above, weather phenomena, including tropical cyclones, played an important part in determining local ambient pollution level. On the one hand, weak winds enhance accumulation of pollutants emitted in the proximity of study region of interest. On the other, stronger winds may transport pollutants from remote places into the study region. In our application, we treat the span of Guangdong province (~350–400 km from HK) as regional with respect to HK. Subsequently, the term *superregional* refers to distances beyond that. Thus, this study appears to be the first to examine the influence of weather in different seasons on local HK pollutant levels. Distinguishing features of this study are (1) the use of an expansive horizontal domain with a fine mesh covering HK, (2) monthlong simulation periods that represent the four seasons, (3) emphasis on PM rather than O_3, and (4) detailed evaluation against observation/measurement data.

[7] Beginning with descriptions of model configurations and construction of emission data in section 2, we report on the performance of the meteorological model in use in section 3. We also characterize the prevailing wind directions in section 3. With well-simulated meteorological fields, a chemical transport model (CTM) produces tracer results that can be directly compared with available observations and/or measurements in the territory; this is expounded in section 4. The previous sections provide a sound foundation to answer the questions of where the air pollution in HK originates, how it evolves, and its dependence on meteorological conditions after emissions are singled out from within PRD or from regions beyond ~350–400 km. Any answer to such questions has undeniable implications on future emission control policies. To estimate the extent of a possible superregional influence on local gaseous and PM levels, we adopt a simple, intuitive approach, called *zero-out*. This involves rerunning the CTM for the 4 months but with emissions partially removed, and results are discussed in section 4.

2. Model Configurations

[8] Figure 1a displays the nested fifth-generation Mesoscale Model (MM5) and CTM grids for our study. Specifically, grid resolutions are 40.5, 13.5, 4.5, and 1.5 km, and the nesting grids are denoted as D1, D2, D3, and D4. D1 aims to cover much of the eastern part of China up to 40°N; D2, Guangdong province in southern China; D3, the Pearl River Delta (PRD) region in middle-south of Guangdong; and D4, Hong Kong, just east of the PRD estuary. The corresponding MM5 grids at each resolution are sufficient to cover the CTM grids with no less than five grid cell-thick buffer on each side, ensuring that undesirable boundary effects of meteorological parameters on CTM grids are reduced to minimum [*Byun et al.*, 1999a]. The size of the 40.5 km D1 grid ensures coverage of vast area of emission sources, so that it can adequately provide background concentrations to the subsequent CTM grids. 20 vertical layers are used in all CTM grids, with 100 mb at the top. The surface layer is approximately 17 m high.

[9] Figure 1b displays monitoring locations of the Hong Kong Environmental Protection Department (HKEPD) Air Pollution Index (API) network and a Hong Kong Observatory (HKO)-maintained wind station. The API network consists of a combined total of 14 ambient and roadside air quality stations, at which hourly data of criteria pollutants are compared with simulations in this study. Hereafter we refer to the API stations as HKEPD stations. The wind station on Waglan Island, southeast of Hong Kong Island, is presumed to represent the background wind for the territory. Wind statistics at this station are displayed in the next section.

[10] Emissions data are constructed as follows. For domains at 4.5 km and 1.5 km resolutions, emission inventories are provided by the HKEPD and, together with MM5 outputs, are processed via SMOKE 2.1 to generate time-varying, gridded emission files. Two major amendments were made to the HKEPD emission inventories. First, under a 2008 study on emission uncertainty in Hong Kong (conducted jointly by HKEPD and Hong Kong University of Science and Technology [HKUST]), power plant emissions were updated with data from the China Electricity Yearbook 2004 (CGDC and CPIC, 2004). Second, on the basis of tunnel measurements conducted by Hong Kong Polytechic University [*HKPU*, 2005], a local PM speciation profile of EC 33.5%, OC 47.5%, $SO_4^=$ 7.5%, NO_3^- 1% and all other ions 10.5% is added for vehicles in HK and the PRD. For domains outside the PRD, i.e., at 40.5 km and 13.5 km resolutions, TRACE-P emissions [*Streets et al.*, 2003] are projected from 2000 to 2004, with growth factors based on *Streets et al.*'s [2007] estimates of 1995–2004 China emissions and studies by *Hao and Wang*

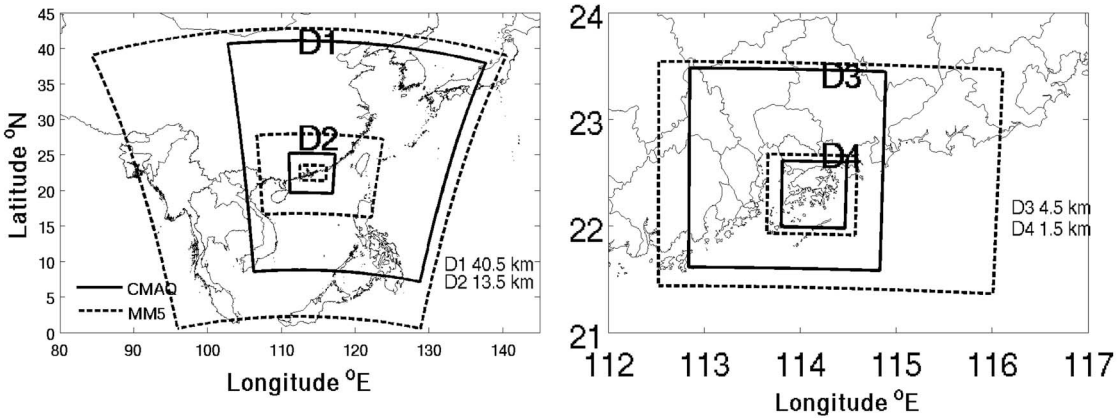

(a)

(b)

Figure 1. (a) MM5 (perforated) and CMAQ (solid) computational domains. (b) HKEPD Air Pollution Index (API) network and a HKO wind station. API network: Yuen Long (YL), Tai Po (TP), Tap Mun (MB), Tsuen Wan (TW), Shatin (ST), Kwai Chung (KC), Sham Shui Po (SP), Mongkok Roadside (MK), Kwun Tong (KT), Central/Western (CW), Central Roadside (CL), Causeway Bay Roadside (CB), Eastern (EN), and Tung Chung (TC). Wind station Waglan Island (WGL).

[2005] and *Heo and Feng* [2005]. The subsequently projected emissions are then combined with the PRD and HK SMOKE emissions for the HK/PRD region. For biogenic emissions, BEIS2 emission factors are used in SMOKE to allocate isoprene, monoterpene, other VOCs, and NO in specified gridded land cover/land use files. In general, the PRD/HK (D3, D4) region is covered by land use data provided by Hong Kong Planning Department [*HKPD*, 2003, Hong Kong 2030: Planning Vision and Strategy Consultancy Study to Analyse Broad Land-Use Pattern of the Pearl River Delta Region, Tech. Paper 5, Final Executive Summary, Baptist University of Hong Kong; available at http://www.pland.gov.hk/pland_en/p_study/comp_s/hk2030/eng/consultants/pdf/Tpaper5.pdf; *Lo et al.*, 2007], while regions outside PRD/HK (D1, D2) are modeled with MODIS annual average land cover satellite pictures.

[11] Meteorology is simulated by the Fifth-Generation National Center of Atmospheric Research/Pennsylvania State University (NCAR/PSU) MM5 version 3.6. On the basis of *Huang*'s [2005] specification, the Grell cumulus parameterization scheme (ICUPA, for D1 and D2 only) [*Grell et al.*, 1994], the medium-range forecast (MRF) planetary boundary layer (PBL) scheme [*Hong and Pan*, 1996], and the Rapid Radiative Transfer Model (RRTM) longwave

Table 1. MM5 Model Performance of Hong Kong Wind Speed in 2004[a]

Obs-Sim All-Wind Statistics (HK Only)											Direction Agreement (>0.5m/s, HK Only)		
Year-Month	Samples (Hour-Stations)	IOA	Corr	RMSE (m/s)	MB (m/s)	ME (m/s)	NMB (%)	NME (%)	MNB (%)	MNE (%)	Year-Month	Samples (Hour-Stations)	IOA_{wdir}
200401	25534	0.78	0.62	2.20	0.18	1.55	4.25	37.43	38.01	62.61	200401	24962	0.94
200404	22182	0.81	0.72	1.89	−0.57	1.25	−14.85	32.79	7.96	44.36	200404	21520	0.94
200407	24656	0.72	0.55	2.53	−0.26	1.70	−6.03	39.22	23.97	56.78	200407	24093	0.94
200410	25780	0.85	0.73	1.76	0.22	1.22	5.80	32.37	31.57	52.48	200410	24994	0.95

[a]IOA, index of agreement; Corr, correlation; RMSE, root mean squared error; MB/ME, mean bias/error; NMB/NME, normalized mean bias/error; MNB/MNE, mean normalized bias/error; IOA_{wdir}, index of agreement for wind directions.

scheme (IFRAD) [*Malwer et al.*, 1997] are employed in MM5 simulations. The number of vertical layers is 34, and thus the number of layer faces is 35, with the top level pressure being 100 mb. In addition to the physics schemes selected, 4-D data assimilation (FDDA) was applied to the MM5 domains. Specifically, analysis data from National Centers for Environmental Prediction Eta Model (NCEP), sampled at 6-hour intervals, are nudged onto the outmost domain (40.5 km resolution). Additionally, surface observational winds are nudged to Hong Kong domain at resolution 1.5 km. Statistics of model performance for our study are reported in section 3.

[12] With emissions and meteorology inputs assembled, preparations are ready to invoke CTM simulations with CMAQ v4.6, in which the Yarmatino mass-conserving advection scheme (yamo, documentation not yet available), aerosol module fourth version [*Reid et al.*, 1987; *Binkowski and Shankar*, 1995; *Binkowski*, 1999; *Binkowski and Roselle*, 2003; *Jiang and Roth*, 2003; *Bhave et al.*, 2004], horizontal diffusion (multiscale) with minimum eddy diffusivity option [*Byun et al.*, 1999b; *CMAS*, 2006], eddy for vertical diffusion, Gear's chemical solver (smvgear) [*Gear*, 1971a, 1971b; *Jacobson and Turco*, 1994; *Ascher and Petzold*, 1998] for the CBIV mechanism, and the Asymmetric Convection Model (ACM) for in-cloud aqueous chemistry [*Pleim and Chang*, 1992; and the Community Modeling and Analysis System (CMAS), 2006 CMAQ Science Update, available at http://www.cmascenter.org/help/model_docs/cmaq/4.5.1/Science_Updates.pdf] are employed.

[13] Starting with CMAQ model profiles, initial conditions are reconstructed after 7-day spin-up runs. The boundary conditions for the outmost domain D1 are extracted from GEOS-Chem-driven (http://www-as.harvard.edu/chemistry/trop/geos/) CMAQ outputs [*Fu et al.*, 2008, 2009], so that background concentrations are made relevant to Asian regions.

3. MM5 Performance and Hong Kong Weather Conditions

[14] The wind station on Waglan Island (refer Figure 1b) in southeastern waters of Hong Kong is presumed, in this study, to provide background wind data that can represent the seasonal weather changes in Hong Kong. Table 1 shows the statistics for the winds over HK automatic wind stations (AWS) during January, April, July, and October 2004. For formulation of the index of agreement, or IOA, refer to *Lu et al.* [1997] and *Barna et al.* [2000]. For all other metrics, consult the U. S. Environmental Protection Agency's [*USEPA*,1991] guidelines. The IOA for wind direction (IOA_{wdir}), due to its vector nature, is reconstructed and described in the Appendix A. In general, the MM5 model performance is similar throughout the year, with the IOA ranging ~0.72–0.85. RMSE ranges ~1.76–2.53 m/s, MB approximately −0.57 to 0.22 m/s, ME ~1.22–1.70 m/s, NMB approximately −14.8 to 5.8%, NME ~32.4–39.2%, MNB ~8–38%, and MNE ~44.4–62.6%. Lower biases occur in April and July (MB −0.57 and −0.26 m/s; NMB −14.85 and −6.03%; MNB 7.96 and 23.97%), while April and October seem to give lower errors (RMSE 1.89 and 1.76 m/s; ME 1.25 and 1.22 m/s; NME 32.79 and 32.37%; MNE 44.36 and 52.48%). The MM5 also agrees well with observational wind directions and gives rise to rather uniform IOA_{wdir} at ~0.94 regardless of seasons. It is worth noting that calculation of IOA_{wdir} takes wind speeds not less than 0.5 m/s. Therefore, with reasonable MM5 results, one can be assured about the subsequent air quality modeling results.

[15] Regarding the wind directions in those months, Figure 2 shows that in January and October, the prevailing wind directions are northeasterly, while easterly and occasional southwesterly winds are seen in April and more southwesterly winds occur in July. The northeasterly winds in January and October are due to the northeasterly monsoon from continental outflows, bringing cold and dry air into the territory. On the other hand, the southwesterly winds are associated with the southwesterly monsoon, bringing humid and unstable air (2004 HKO data, available at http://www.weather.gov.hk/wxinfo/pastwx/wms.htm). As revealed later, these weather patterns play key roles in local ambient pollution levels.

4. Model-Observation Comparisons

[16] To clarify the layout of the HKEPD station network (Figure 1b), we describe the local features of the territory. As shown in Figure 1b, the territory consists of Hong Kong Island in the south, Kowloon Peninsula immediately north of it, separated by the narrow Victoria Harbor, with Lantau Island in the southwest. The primary commercial area is concentrated on both sides of Victoria Harbor, namely, on northern part of Hong Kong Island and the southern tip of Kowloon Peninsula. Central/Western, Central Roadside, Causeway Bay Roadside, and Eastern stations are on Hong Kong Island, while Sham Shui Po, Mongkok Roadside, and Kwun Tong are in downtown Kowloon. Separated by a mountain range from the downtown area, the rest of the peninsula is called the New Territories and is mainly moun-

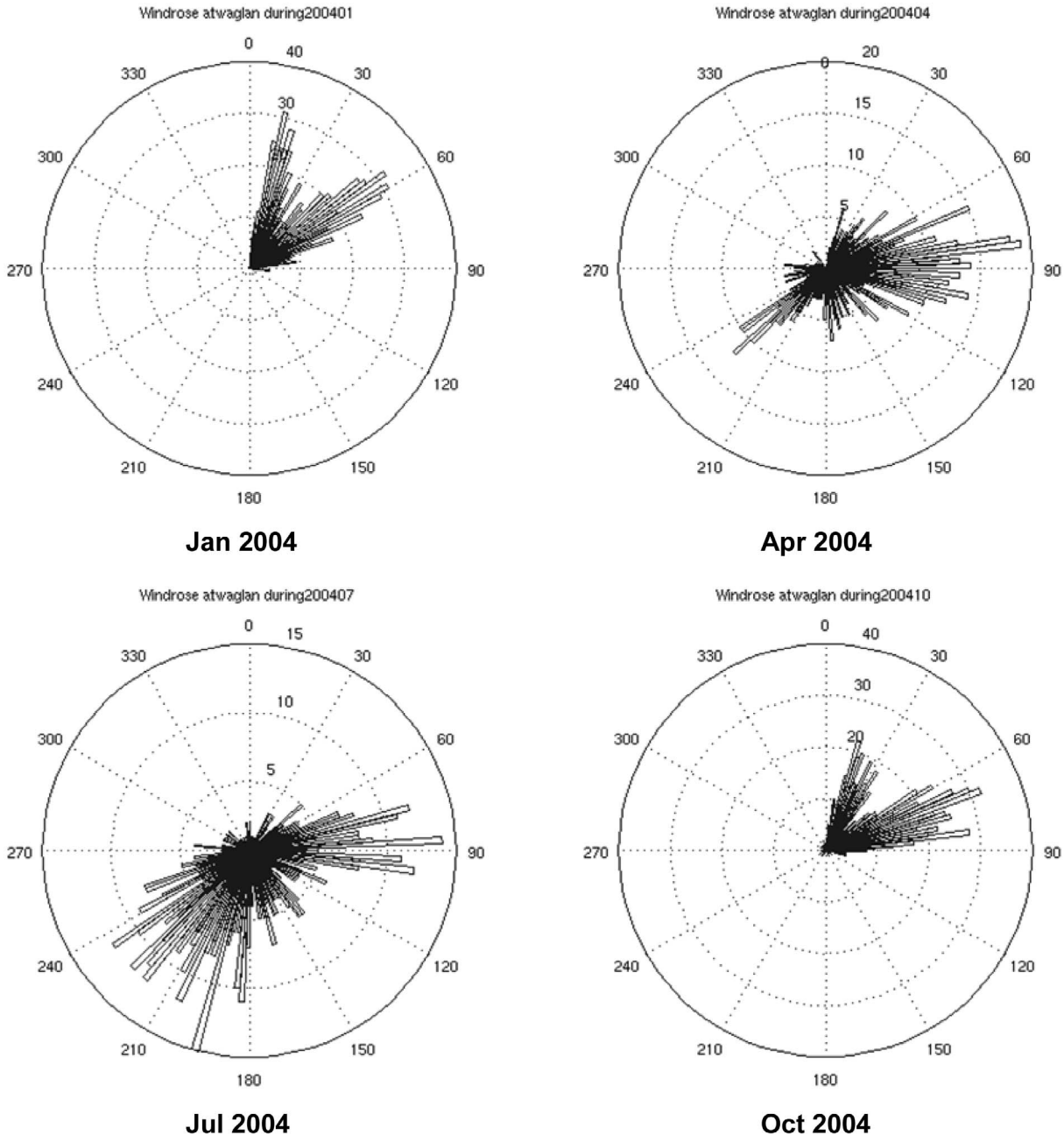

Figure 2. MM5 wind rose for January, April, July, and October 2004 at Waglan Island wind station (see Figure 1b).

tainous, with the exception of the northwestern area. The highest mountain is located in central New Territories, surrounded by scattered but populous townships. HKEPD stations in Shatin and Tai Po are on the east side, Kwai Chung and Tsuen Wan on the southwestern side, and Yuen Long on the northwestern side. In addition, two remote HKEPD stations are designed to keep track of background concentration levels: Tap Mun in the northeast and Tung Chung on Lantau Island.

[17] Two sets of observations/measurement data are employed to evaluate the model performance. The first set comes from real-time hourly observational data recorded at HKEPD stations (Figure 1b). Species of interest include PM sulfate, its precursor SO_2, $PM_{2.5}$, PM_{10}, ozone, and nitrogen oxides. We refer to this dataset as EPDHOUR. The second data set consists of speciated PM measurements [*Yuan et al.*, 2006], sampled at 6-day intervals over the same period, at six HKEPD ambient stations: Central/Western, Kwun Tong, Sham Shui Po, Tung Chung, Tsuen Wan, and Yuen Long. We denote this dataset EPD6DAY, which consists of PM_{10} species sulfate, OC, EC, ammonium, nitrate, chloride, sodium, and other ions.

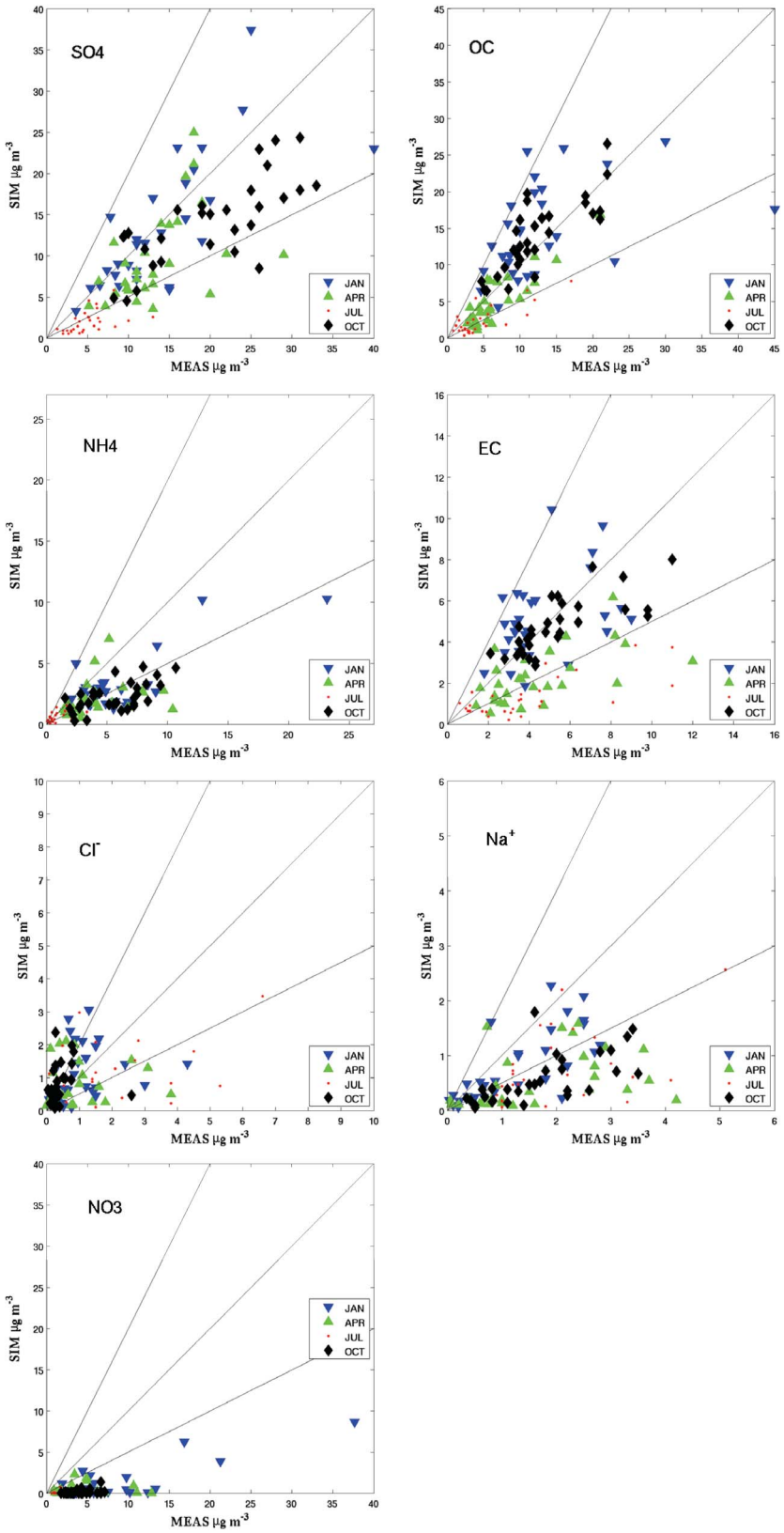

Figure 3. Scatterplots of SO_4, OC, NH_4, EC, Cl, Na, and NO_3 in January, April, July, and October 2004. EPD6DAY versus simulation.

Table 2. Model Performance Compared to EPD6DAY PM_{10} Species in January, April, July, and October 2004

Species	Month-Year	Jan-04	Apr-04	Jul-04	Oct-04
Sulfate	MeanObs ($\mu g/m^3$)	14.02	13.46	4.88	19.42
	MeanSim ($\mu g/m^3$)	13.47	9.63	1.96	13.68
	IOA	0.85	0.61	0.52	0.69
	NMB (%)	−3.96	−28.44	−59.83	−29.52
	NME (%)	26.42	37.00	59.83	33.77
OC	MeanObs ($\mu g/m^3$)	14.11	7.13	4.44	12.15
	MeanSim ($\mu g/m^3$)	15.31	5.69	2.45	14.13
	IOA	0.62	0.86	0.63	0.79
	NMB (%)	8.49	−20.18	−44.92	16.31
	NME (%)	44.64	31.31	55.69	27.96
EC	MeanObs ($\mu g/m^3$)	4.60	4.59	3.86	5.34
	MeanSim ($\mu g/m^3$)	5.10	2.52	1.34	4.86
	IOA	0.64	0.57	0.49	0.66
	NMB (%)	10.84	−45.18	−65.27	−8.91
	NME (%)	38.92	47.51	66.47	23.59
NH_4	MeanObs ($\mu g/m^3$)	5.63	4.32	0.75	5.48
	MeanSim ($\mu g/m^3$)	3.08	2.02	0.56	2.23
	IOA	0.70	0.51	0.65	0.53
	NMB (%)	−45.18	−53.32	−24.45	−59.30
	NME (%)	48.33	57.88	55.49	59.94
NO_3^-	MeanObs ($\mu g/m^3$)	7.88	4.07	1.76	4.11
	MeanSim ($\mu g/m^3$)	1.09	0.33	0.09	0.13
	IOA	0.48	0.43	0.35	0.35
	NMB (%)	−86.14	−91.85	−95.01	−96.76
	NME (%)	86.14	91.85	95.01	96.76
Cl	MeanObs ($\mu g/m^3$)	1.35	0.81	1.65	0.40
	MeanSim ($\mu g/m^3$)	1.10	0.67	1.02	0.73
	IOA	0.28	0.49	0.61	0.39
	NMB (%)	−19.03	−17.43	−38.31	82.78
	NME (%)	78.98	83.99	68.03	122.36
Na	MeanObs ($\mu g/m^3$)	1.28	1.60	1.97	1.71
	MeanSim ($\mu g/m^3$)	0.82	0.51	0.76	0.55
	IOA	0.77	0.54	0.54	0.55
	NMB (%)	−36.08	−68.41	−61.64	−67.93
	NME (%)	44.82	72.04	61.94	68.56

4.1. Overall Performance

[18] Since our modeling study is still in the preliminary stage, model verification seems to be our first priority. Bearing in mind that PM affects HK a lot, we first report the model performance metrics of PM on the basis of the hourly data and EPD6DAY data. Then we go through each of the PM species from the EPD6DAY data in the hope of identifying possible causes of good or less satisfactory simulations. This subsection ends with metrics for the hourly model/observation data of criteria pollutants PM_{10}, $PM_{2.5}$, SO_2, and NOx.

[19] The scatterplots of EPD6DAY versus CMAQ (Figure 3) show better model performance in $SO_4^=$, OC, and EC, and worse performance in NO_3^-. As indicated earlier, PM speciation profile for Hong Kong vehicles replaces a default one in SMOKE emission processor. It is expected then that the OC and EC are modeled reasonably well in terms of concentration levels and portion of PM composition, and this is demonstrated later. From Table 2, maximum normalized mean error is 56% for OC and 66% for EC, which is comparable to *Eder and Yu*'s [2006] evaluation over the USA (68% for OC and 58% for EC). Normalized mean bias can get as far as −45% for OC and −65% for EC, which is relatively moderate when compared to the *Simpson et al.* [2007] report on European study, in which the total carbon was underestimated by ~3–5 times.

[20] In contrast to OC and EC, underprediction in April occurs in sulfate, ammonium, chloride, sodium, and nitrate, July in all the species, and October in sulfate, ammonium, sodium, and nitrate. Table 2 conveys the information quantitatively, clearly showing a significant negative bias occurring in April and July for those PM species.

[21] The model performance of the meteorology (Table 1) shows that July has lower index of agreement (IOA) and higher errors in wind speed. Thus, the July meteorology may significantly contribute to the PM underprediction.

[22] Ammonia emissions seem insufficient to supply the observed levels of ammonium. Underestimation of chloride and sodium is possibly due to CMAQ, in which sea salt is the only emission source. Unconsidered other sources include gaseous HCl, which may originate from biomass burning [*Andreae et al.*, 1996; *Khan et al.*, 2009], coal burning, and/or waste incineration [*McCulloch et al.*, 1999]. Since April falls in the season of biomass burning, those alternative sources of chloride may make up for the model underestimation. Sodium in fine modes also naturally occurs in biomass [*Khan et al.*, 2009].

[23] Nitrate is grossly underestimated for two possible reasons. First, as we see later, nitrogen oxide emissions are underestimated. Second, CMAQ 4.6 has not implemented the formation of coarse-mode nitrate, which consists of two pathways: reactions between gaseous HNO_3 and sodium chloride and between HNO_3 and calcium carbonate. It is hoped that modeling of gaseous and PM nitrogen compounds can be improved with the addition of these reactions.

[24] We also look at PM composition in the EPD6DAY measurement and CMAQ outputs in the hope of assessing emission data processing and the AQ model output.

[25] Figure 4 shows the stacked percentage bars of PM_{10} composition at six HKEPD stations. For each month representing a season, a pair of the stacked bars consisting of observed PM data from EPD6DAY (left) and simulated PM outputs (right) is displayed. There is no measurement at Sham Shui Po in January, so stacks are made only for April, July, and October. From Figure 4 we can see that measured PM composition is rather uniform throughout the year, though total concentration levels are not necessarily so. The model also exhibits annual uniformity in PM composition.

[26] Furthermore, the model seems to match the fractions of $SO_4^=$, OC, and EC quite well, to within 10% of measurements, in which the measured $SO_4^=$, OC, and EC make up approximately 35%, 10%, and 25% of total PM mass, respectively. The major differences occur in nitrate and other unspecified PM species. While the nitrate fraction is barely visible from stack bars of simulations, the unspecified PM fraction is >30%, much higher than in observed PM measurements. The ammonium fraction, either with nitrate or with sulfate, especially in April and October, is also underestimated by about half, According to *Streets et al.* [2003], the major sources of NH_3 in China are fertilizers (45%) and animals (38%), which are indicated in the same paper as being highly uncertain sources. As a result, it is quite probable that emissions from those sources are still well underestimated. The low modeled nitrate problem, as stated before, is probably caused by inadequate NOx emissions and the absence of the formation of coarse-mode nitrate.

[27] In EPD6DAY data, the category "other" includes inorganic ions such as Al, As, Ca, Cd, Fe, K, Mg, Mn, Ni,

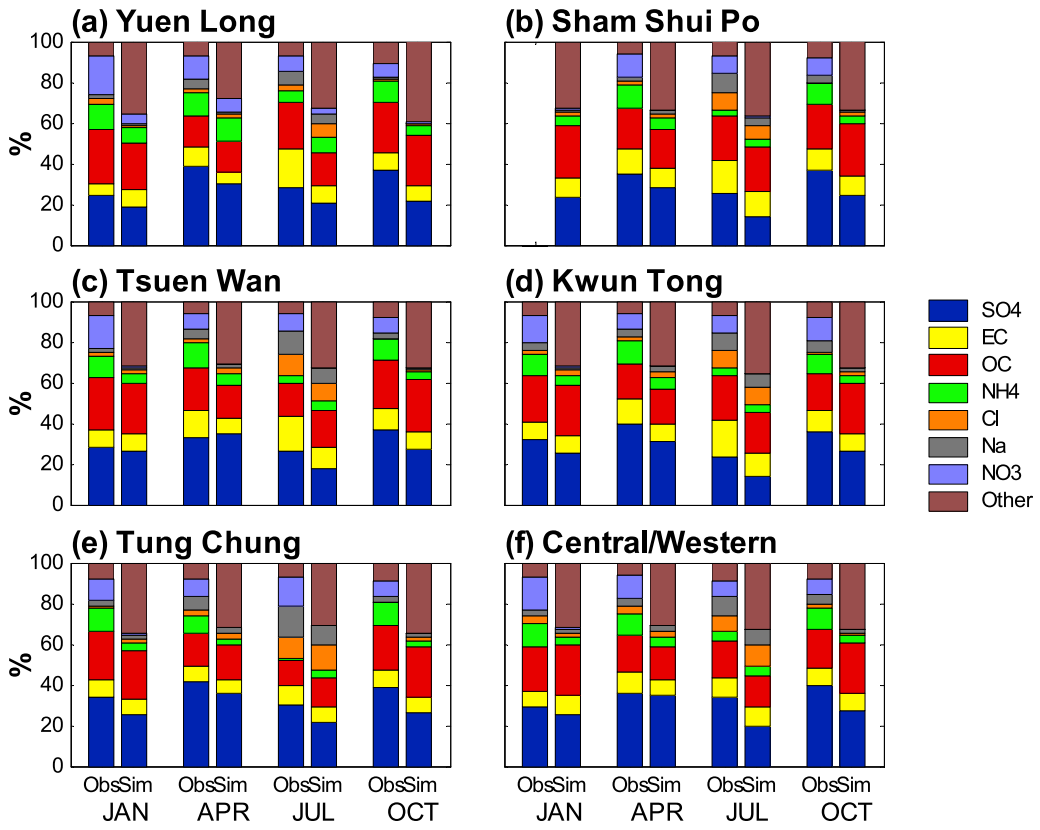

Figure 4. Stacked percentage bars of PM_{10} composition at (a) Yuen Long, (b) Sham Shui Po, (c) Tsuen Wan, (d) Kwun Tong, (e) Tung Chung and (f) Central/Western. At each EPD station, four pairs of stacks occur in January, April, July, and October 2004. In each pair of stacks, left is EPD6DAY, and right are simulations.

Table 3. Hourly Model Performance of Criteria Pollutants Over All HKEPD Stations

Pollutant Prediction Performance 2004 Over All HKEPD Stations					
Species	Metrics	Jan	Apr	Jul	Oct
SO_2	MeanObs ppbV	7.5	10.1	7.5	9.0
	MeanSim ppbV	7.3	6.3	5.0	7.0
	IOA	0.49	0.55	0.41	0.47
	NMB %	−3.5	−37.5	−33.5	−22.5
	NMGE %	65.5	68.6	83.5	48.8
$PM_{2.5}$	MeanObs μg/m3	51.7	46.9	22.4	66.5
	MeanSim μg/m3	46.1	22.6	5.9	43.8
	IOA	0.63	0.53	0.42	0.55
	NMB %	−11.0	−51.9	−73.9	−34.1
	NMGE %	36.9	56.0	77.6	38.1
PM_{10}	MeanObs μg/m3	67.6	59.4	28.4	88.3
	MeanSim μg/m3	56.8	29.7	11.6	53.9
	IOA	0.63	0.53	0.38	0.51
	NMB %	−16.0	−49.9	−59.2	−38.9
	NMGE %	37.3	54.2	67.8	41.9
O_3	MeanObs ppbV	21.1	22.9	8.7	37.9
	MeanSim ppbV	37.7	26.3	15.6	43.6
	IOA	0.58	0.74	0.48	0.75
	NMB %	77.1	14.5	76.3	14.8
	NMGE %	91.1	60.8	112.6	40.8
NOx	MeanObs ppbV	93.0	91.6	82.0	96.5
	MeanSim ppbV	30.4	37.4	39.5	35.9
	IOA	0.52	0.52	0.51	0.52
	NMB %	−67.3	−59.2	−51.8	−62.8
	NMGE %	70.3	65.4	65.8	66.8

Pb, and V. Clearly their mass is insignificant compared to the major PM species. In the model output, on the other hand, the category "other" consists of soil, coarse particles, and unidentified accumulation mode PM. In fact the unidentified PM makes up 80% of the "other" mass (not shown), thus introducing a very large uncertainty. This is likely related to the accuracy of PM speciation in each individual source category as discussed by *Appel et al.* [2008]. Additionally, most sources in HK/PRD assume USEPA AP42 SPECIATE speciation profiles [*USEPA*, 2000], except for on-road motor vehicles, marine sources, and power plants. According to

Table 4. Model Performance of Hourly Sulfate at Yuen Long and Tsuen Wan in April, July, and October 2004

EPD Station	Model Performance 2004				
		Jan	Apr	Jul	Oct
Tsuen Wan	Mean Obs μg/m^3	N.A.	9.2	3.6	14.3
	Mean Sim μg/m^3	N.A.	11.2	2.4	13.5
	IOA	N.A.	0.62	0.42	0.53
	NMB %	N.A.	13.7	−34.8	−5.4
	NMGE %	N.A.	54.4	61.6	45.1
Yuen Long	Mean Obs μg/m^3	N.A.	13.2	2.5	17.6
	Mean Sim μg/m^3	N.A.	11.6	2.9	14.8
	IOA	N.A.	0.55	0.30	0.65
	NMB %	N.A.	−12.0	1.6	−15.9
	NMGE %	N.A.	55.2	101.5	34.5

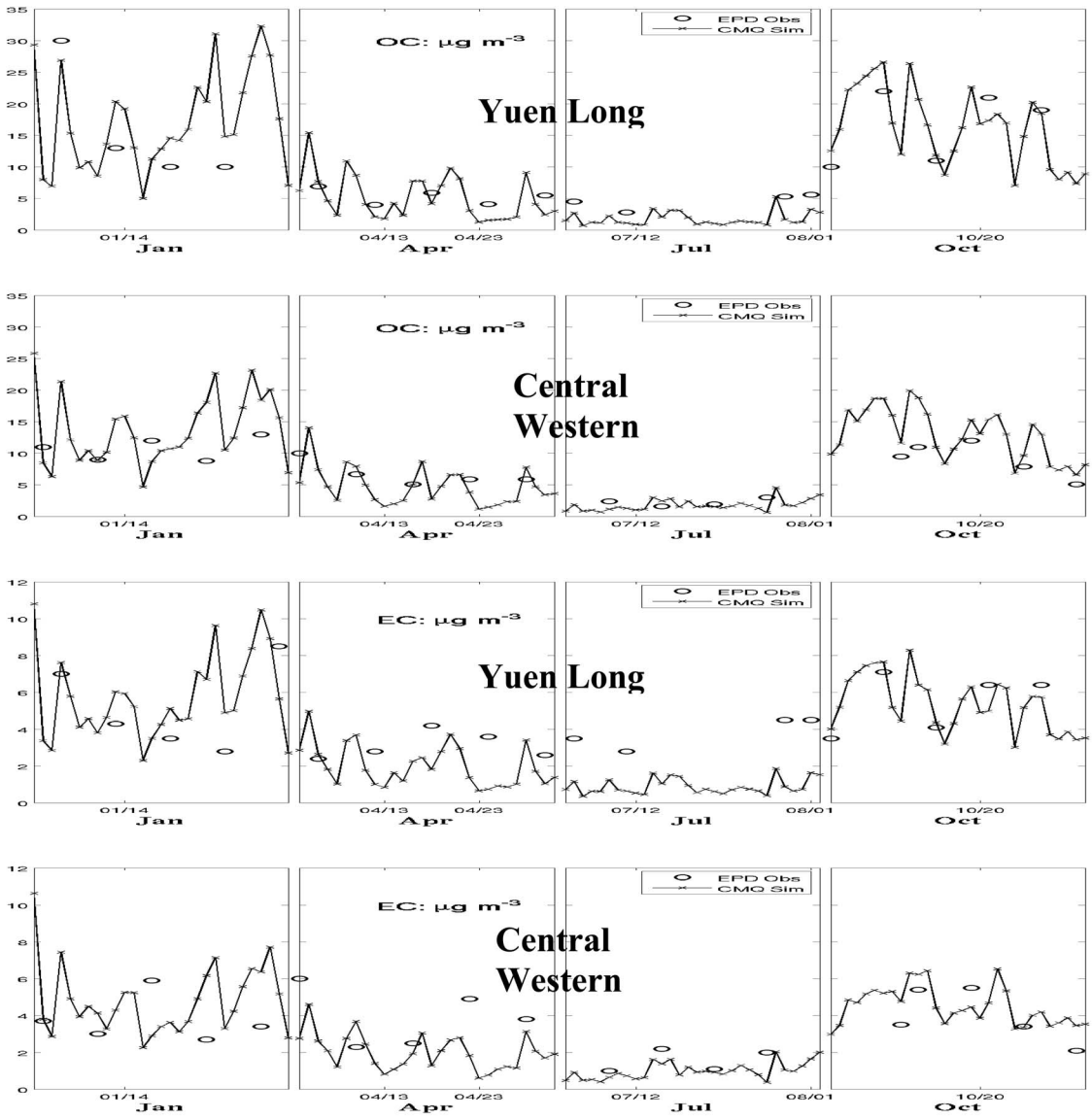

Figure 5. Daily averaged OC and EC at Yuen Long and Central/Western in January, April, July, and October 2004. Circles, six-daily sampled PM_{10} measurements (EPD6DAY hereafter); lines, simulations.

Reff et al. [2009], ionic species are also included in speciation profiles for emission modeling.

[28] Tables 3 and 4 display model performance metrics for hourly data, EPDHOUR, of criteria pollutants in the four seasons. In general, SO_2 is moderately underestimated in most seasons except for January (bias −3.5% to −37.5%), $PM_{2.5}$ and PM_{10} significantly in those seasons (bias −11% to −73%, and −16% to −59%, respectively), and NOx grossly in all seasons (bias −52% to −67%). In contrast, ozone is overestimated in all four seasons, especially in January and July (bias +77% and +76%, respectively). The results are consistent with the EPD6DAY-model comparison. Together, they show that underprediction of most pollutants takes place in April, July, and October. We look closely at seasonal variations at individual sites.

4.2. Seasonal Variations

[29] Figure 5 plots time series of OC and EC, at 6-day intervals, at Yuen Long and Central/Western. OC level in the model time series at Yuen Long is quite close to the measurements. The measurements indicate gradual decrease across April and July, which is also truly reflected in the model time series. The model finishes with excellent match in October, some points matching almost exactly with measurements on October 15 and 27. Similar behavior is seen in Central/Western's OC. Performance of EC is similar to that of OC, except for Yuen Long in April and July, in which the model underestimates the measurement quite significantly. In both simulations and observations, OC varies between ~2 and 30 $\mu g/m^3$ and between EC ~1 and 8 $\mu g/m^3$. Season-to-season variation, with higher concentrations in January and October than in April and July, is more prominent in OC than in EC. Also, OC and EC levels are

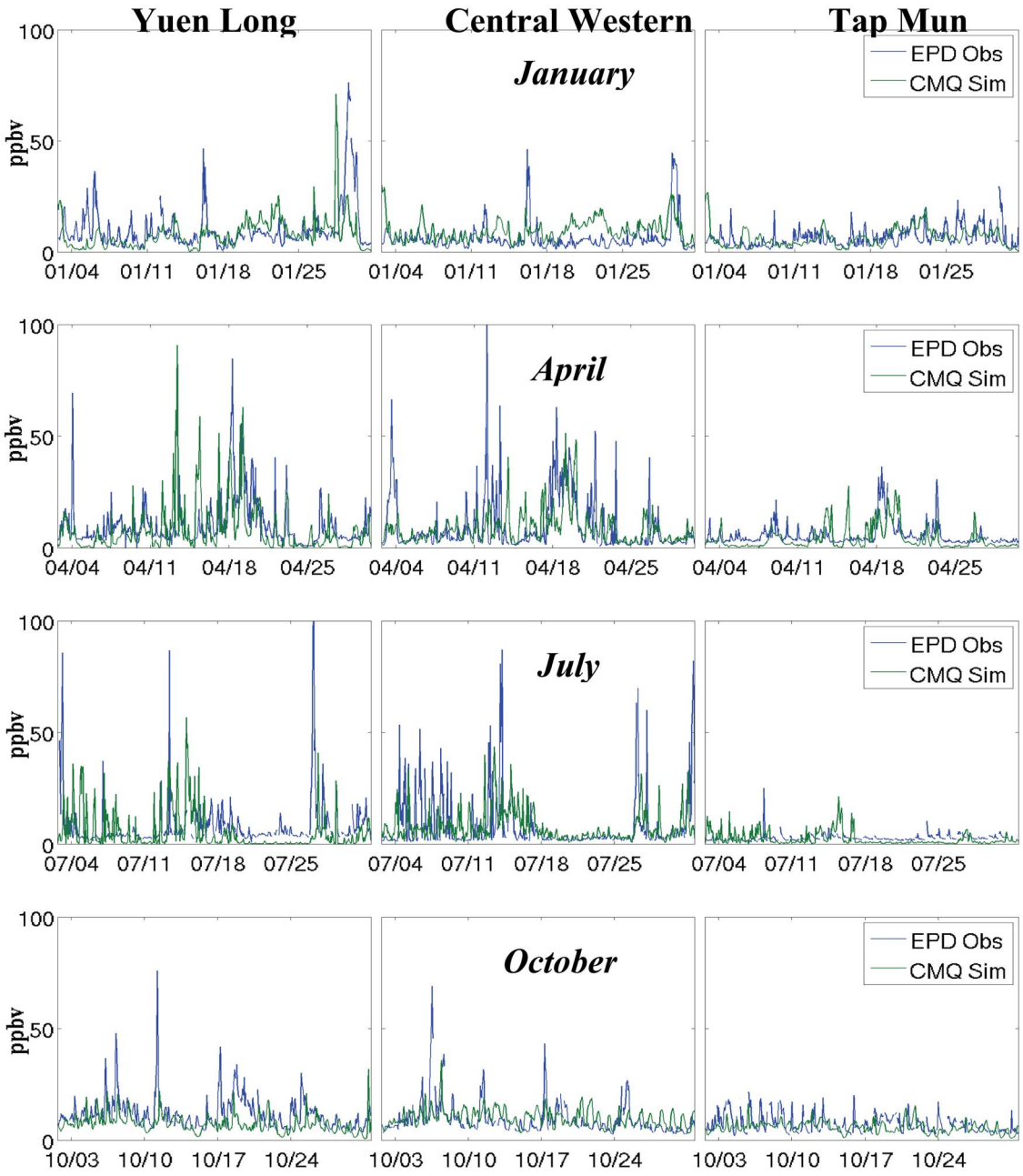

Figure 6. Same as Figure 3, except for SO_2 at Yuen Long, Central/Western, and Tap Mun in January, April, July, and October 2004.

higher in Yuen Long than in Central/Western, hinting at regional influence from neighboring Shenzhen where power plants, on-road traffic, and industrial production are very active. The spatial variations are discussed in depth later.

[30] The observed SO_2 exhibits a certain kind of seasonality for 2004. Figure 6 shows that SO_2 at Yuen Long and Central/Western fluctuates with spikes in April and July and varies relatively smoothly in January and October, possibly because there are power plants west and southwest of Yuen Long and there is one south of HK Island. In April and July, winds have southerly components so that the two HKEPD sites become downwind of these sources. On the other hand, Tap Mun exhibits less obvious SO_2 seasonal variations, with SO_2 levels slightly lower in July. CMAQ seems to capture the underlying SO_2 trends as well as most of the spikes in April and July at the three sites, with the exception of Yuen Long and Tap Mun during 18–25 July.

[31] Figure 7 shows that at both ends of the territory, east (Tap Mun) and west (Tung Chung), $PM_{2.5}$ trends are similar, with higher average levels in January and October, and the lowest in July, alluding to an evident seasonal cycle. The similarity in different areas of the territory also suggests that local sources seem to play less significant roles in the $PM_{2.5}$ level. CMAQ is able to capture the seasonality, although it underpredicts the trends in April and July. According to *Kim Oanh et al.* [2006], biomass burning activities occur from

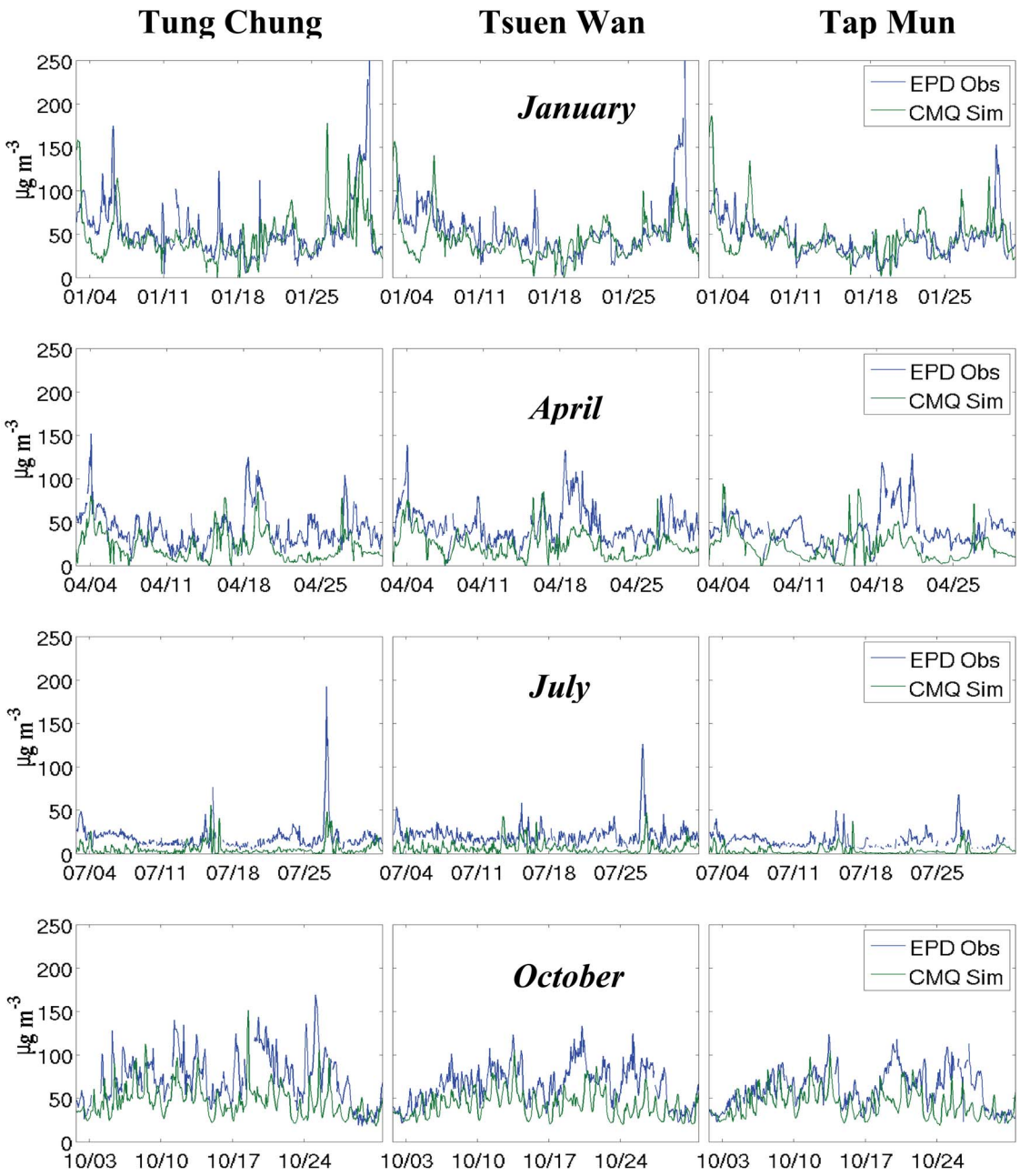

Figure 7. Same as Figure 4, except for $PM_{2.5}$ at Tung Chung, Tsuen Wan, and Tap Mun.

October to April, mainly in Southeast and East Asia. Therefore the model-observation discrepancies in April are possibly due to the missing biomass burning sources, currently not included in our emission inventories. On the other hand, the model performs better in January and October in terms of peak-matching and trend-following skill (Figure 7), while the two months are dominated by the northeasterly monsoons.

[32] Although the overall concentration levels in July's observed data are low, the model underpredicts the $PM_{2.5}$ quite considerably. In the GEOS-Chem boundary conditions ingested into the simulations, the highest concentrations of NO_3^-, EC, and $SO_4^=$ are along the northern boundary of D1 (covering northern China), at ~1.32 $\mu g/m^3$, 0.38 $\mu g/m^3$, and 6.4 $\mu g/m^3$, respectively. Although the values seem low, it remains inconclusive whether this causes underestimation of pollutants in the innermost domain.

[33] In general, ozone trends are followed well in all four months at downtown Central/Western, in April and July at downwind Tung Chung, and in April and October at upwind Tap Mun (Figure 8). The satisfactory O_3 performance is also associated with better NOx modeling at Tung Chung and Central/Western stations in their corresponding months (Figure 9), suggesting that the amount of VOC/NOx emissions are about right in these periods at the two observational sites. On the other hand, overestimations of O_3 occur in January at Tung Chung and Tap Mun, and in July at Tap

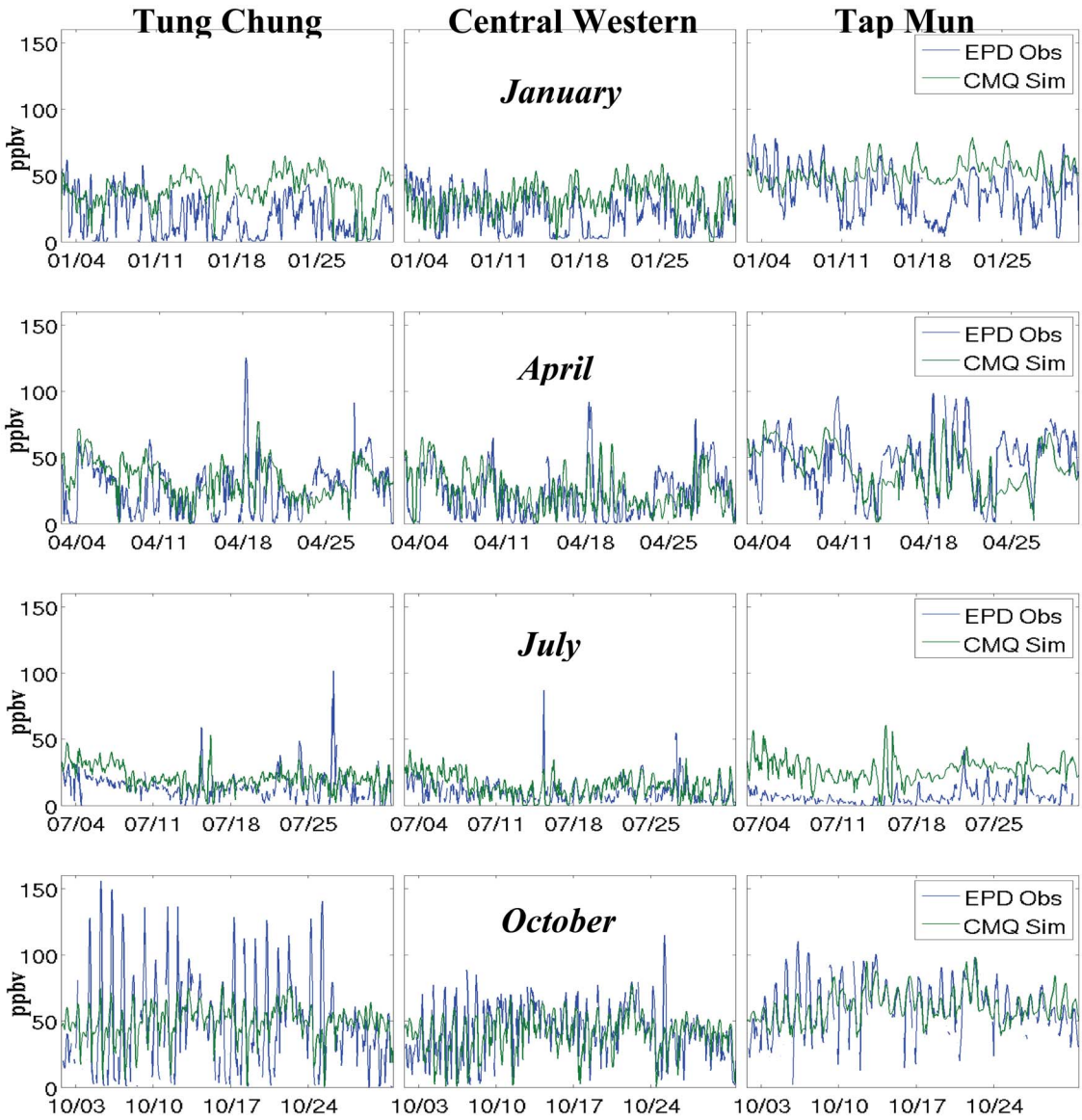

Figure 8. Same as Figure 4, except for O_3 at Tung Chung, Central/Western, and Tap Mun.

Mun (Figure 8). NOx trends are underestimated and stationary at Tung Chung and Central/Western during the corresponding periods (Figure 9). However, the highly varying observational ozone at Tung Chung, poorly captured by the model, is not easily explained despite considering factors ranging from air temperature [*Kelly and Gunst*, 1990], O_3-favorable VOC/NOx ratios of ~7–10 [*Chang et al.*, 1989] or O_3-unfavorable ratios of <5.5 [*Seinfeld and Pandis*, 1998]. What distinguishes Tung Chung from other observational stations is that it has lower on-road traffic density and often becomes downwind to the rest of HK territory in easterly winds.

[34] Figure 10 shows hourly time series of modeled and observed sulfate. Except for January, observations are available for the other three months. Considerably lower concentration level occurs in both modeled results and observations in July than in other months. April case exhibits larger variations across the two stations, while October case displays similar temporal variations across them. The model performs quite well in July and October, but tends to underpredict high episodes at Yuen Long and to overestimate the trend at Tsuen Wan.

[35] In summary, the model is capable to reproduce higher concentration levels in January and October and lower levels in July, although PM species are often underpredicted and O_3 overpredicted. Thus the modeled meteorology is capable of capturing the seasonal variations.

4.3. Spatial Variations

[36] While Tables 2 and 3 displays the average concentration levels for each season in model and observations, model performance is evaluated better if distributions across the API stations are shown for both model results and observations/measurements. To compare the spatial distribution of a given pollutant, we first take the temporal mean at each API site within each of the four seasons, then we

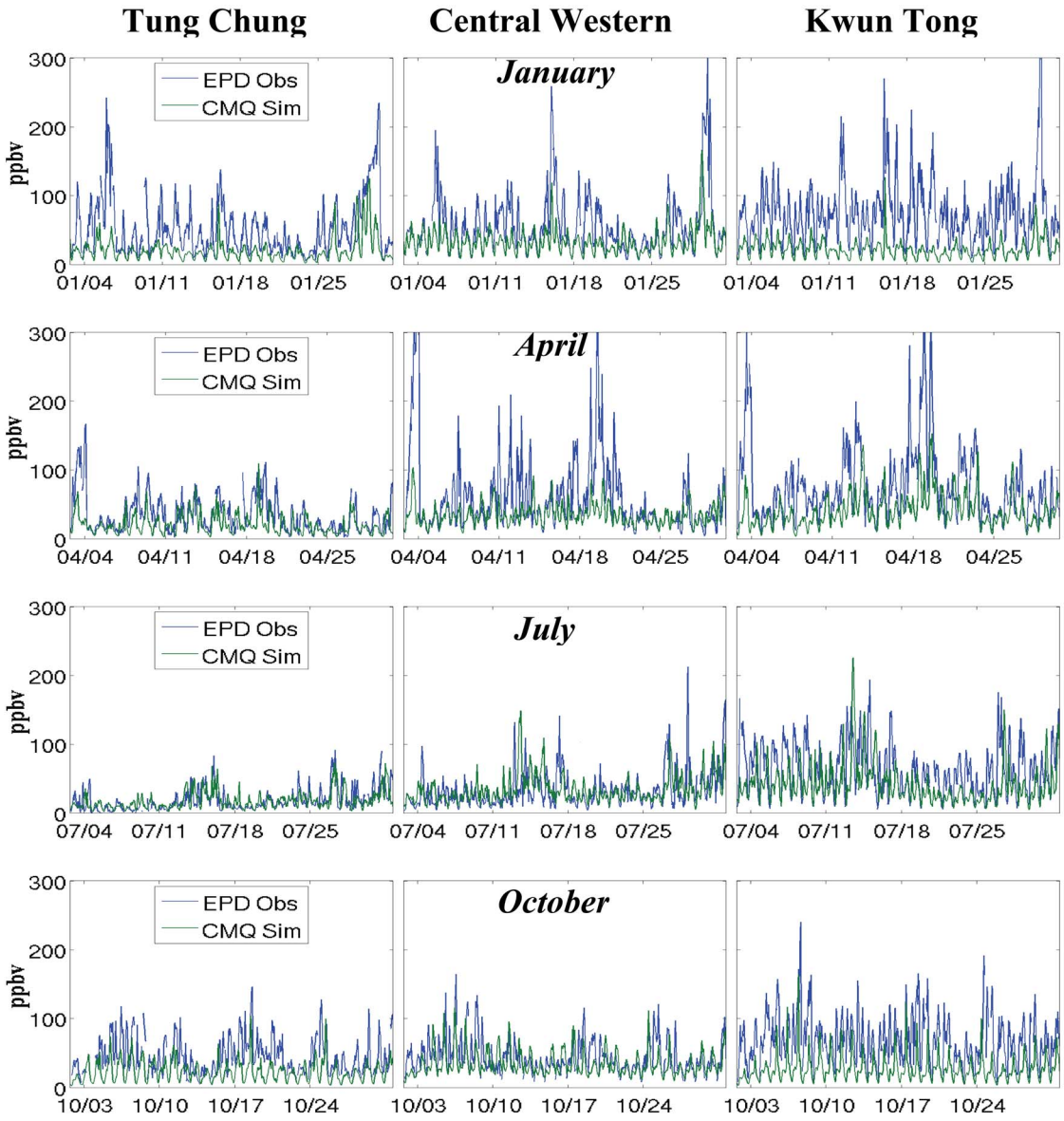

Figure 9. Same as Figure 4, except for NOx at Tung Chung, Central/Western, and Kwun Tong.

average the values over all the API sites. Subsequently, the percentage difference between each API site and the all-site average is computed. The arithmetic is independently applied to observational/measurement data and modeled results, and spatial plots from both datasets are compared side-by-side. On the basis of the API hourly observations of O_3, PM_{10}, and EPD6DAY sulfate, the spatial distribution plots for all seasons are shown in Figures 11–13, respectively. In each figure, bar plots are also placed next to the spatial plots. Individual sites are arranged from west to east so that percentage values in the bar plots can be checked against those on the spatial plots. Red bars denote the percentage difference in the modeled results, while blue ones are based on observations.

[37] In Figure 11, the observational bars of O_3 increase from west to east in January, are below the all-site average in central sites in April, and exhibit mixed anomalies in central sites in July and October. By same sign of anomaly, it means percentage differences are either positive or negative in both the model and the observations. Opposite signs mean one is positive and one is negative. Then the model predicts the same sign of anomaly at four of eight sites in January, six of nine in April and July, and four of nine in October. However, in the October case, the opposite signs at the sites vary between −15% and +15% from the mean. This indicates that uniformity around the central (downtown) sites is captured by the model quite well in October. Significantly high percentage differences occur in the eastmost site Tap Mun (MB) in January, April, and October, but the model is able to capture the peaks in those seasons. The peak in the westernmost site Tung Chung (TC) is also predicted by the model. Since both TC and MB are downwind background sites, the spatial distribution of observational O_3 seems reasonable in the way that lower levels

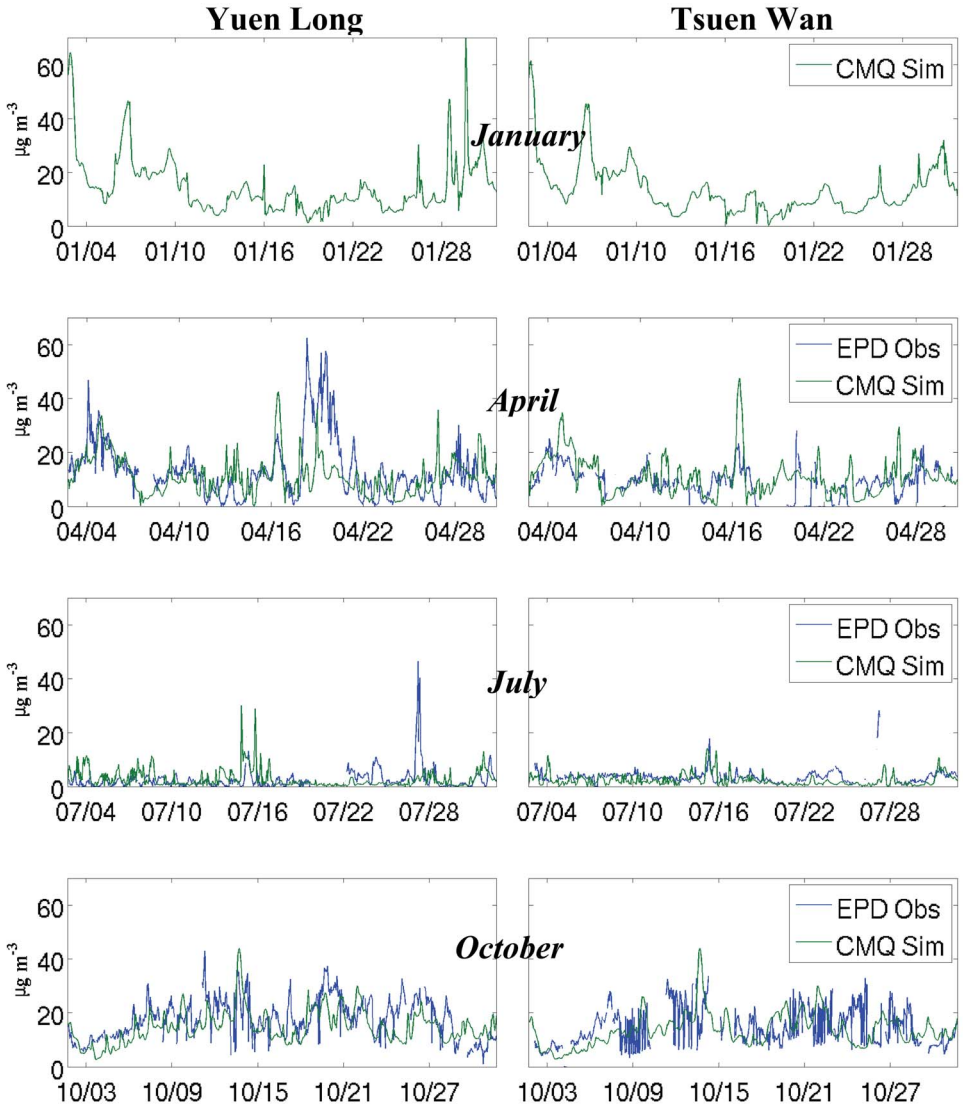

Figure 10. Hourly time series of PM sulfate at Tsuen Wan and Yuen Long in January, April, July, and October 2004. Blue, observations; green (and/or red marks), simulations.

around downtown areas correspond to possible titration with vehicle NOx. Thus the model can also reproduce the spatial patterns.

[38] Similar comparison for PM_{10} is shown in Figure 12. The observed PM_{10} exhibits a decreasing trend when moving eastward in January, although values at all sites deviate only mildly from the average. Small variations (less than or equal to ±15%) occur in April and October, but large variations occur in July. For January, April, and October, small deviations imply uniformity of PM_{10} concentrations across the API sites, and hence suggest regional contributions for these seasons. Larger variations in July, on the other hand, seem to suggest contributions in this season are from localized sources near individual sites. Additionally, the all-site average concentration is considerably lower in July than in other seasons, and therefore larger variations can occur. The below-average values at TC and MB in July imply low background concentrations and therefore strengthen the possibility of local PM contributions. The model predicts same sign of anomaly at six of nine sites for January case, seven of nine for April, four of nine for July, and six of nine for October. The less satisfactory performance in July is perhaps related to poorest modeled meteorology for this month, where the IOA is lowest compared to the other three months (Table 1). In addition, emission estimates around the downtown areas certainly need to be improved.

[39] Figure 13 displays the similar comparison for speciated sulfate from EPD6DAY samples. Of the five available sites, three are predicted for same sign of anomaly in January, four in April and July, and all in October. In January and October, the measured $SO_4^=$ exhibits a decreasing trend from northwest to southeast, which is reproduced by the model. The below-average percentage in TC in January and July is also captured by the model. Larger variations are seen in the modeled percentage for April and July, possibly because the model concentration level is lower than in January and October. The October case seems to be best predicted, whether in regard to the sign of anomaly and in

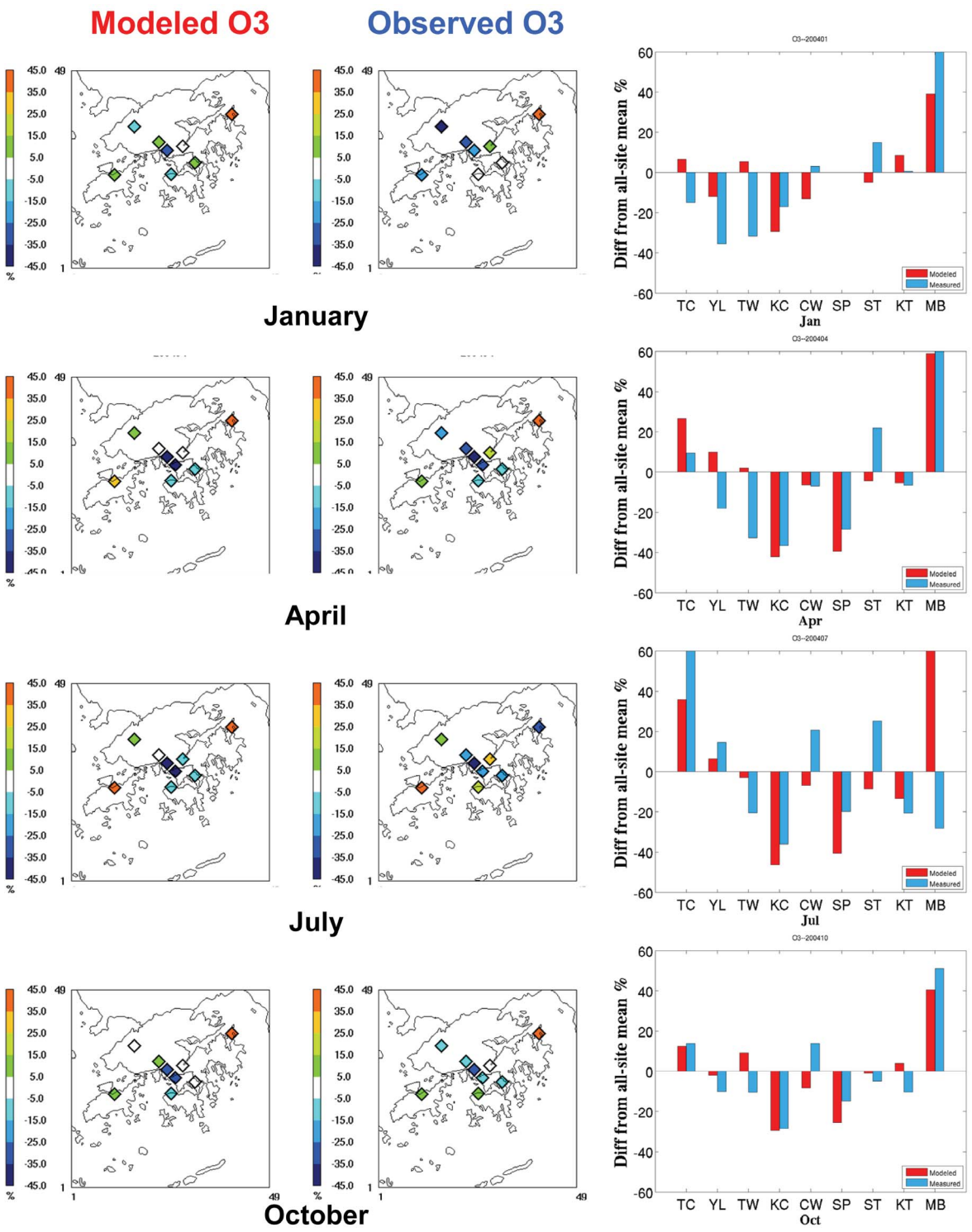

Figure 11. Percentage difference from all-site average of ozone. (left) Model; (middle) observations; (right) bar plots at the individual sites from west to east. See Figure 1b for station names.

deviations from all-site means. The peaks at Yuen Long in the four seasons suggest possible PRD influence that would affect less all other monitoring sites. Although we are aware of a possibility of local land-sea breeze effect around PRD estuary [*Lo et al.*, 2006], a further in-depth study is certainly required in the near future.

[40] In summary, model O_3, PM_{10}, and sulfate captures the spatial patterns well in October. O_3 is less satisfactory in January and July, and PM_{10} in July. The model appears to have more accuracy in capturing background concentrations, but less accuracy in capturing the high spatial variations in urban sites.

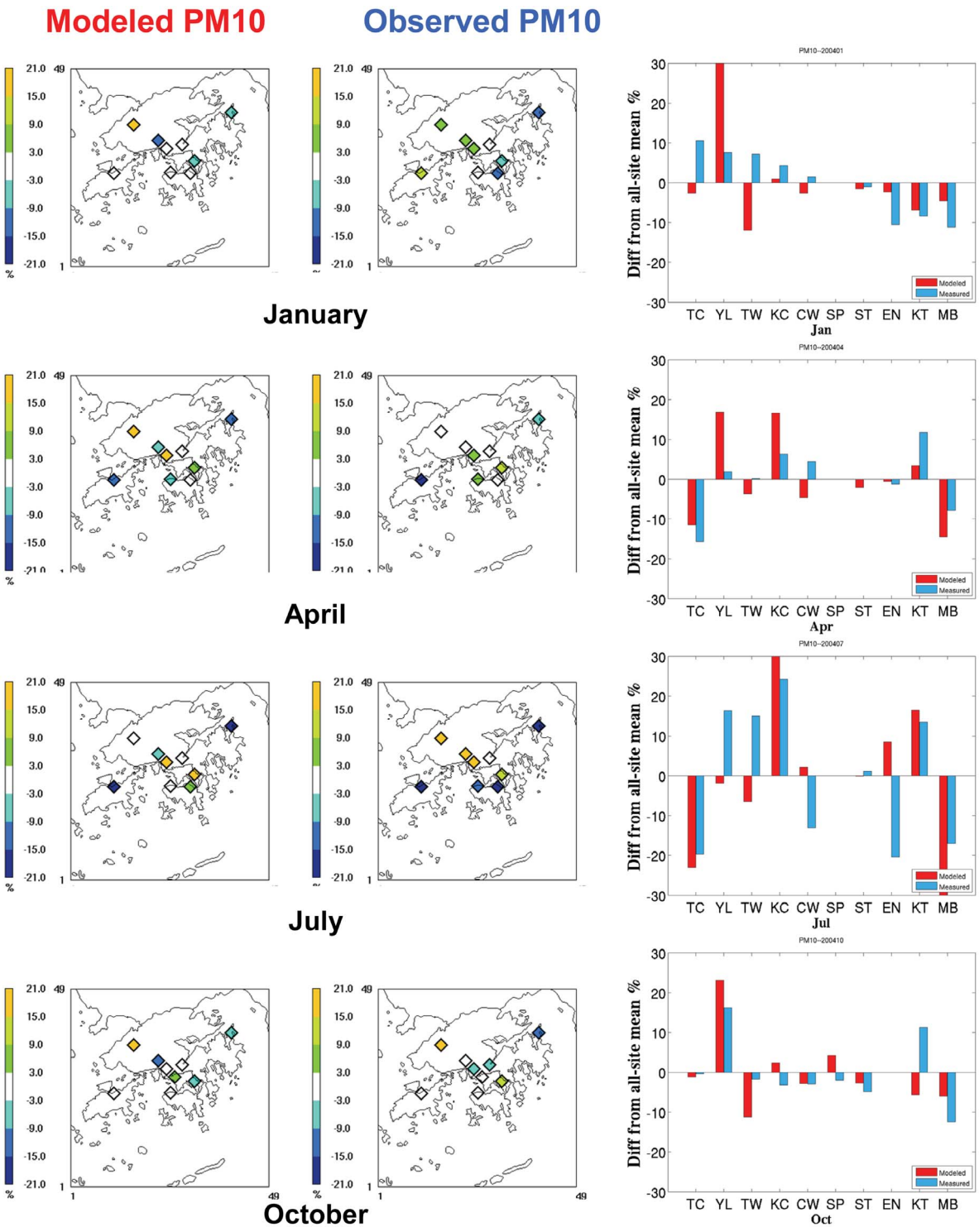

Figure 12. Percentage difference from all-site average of PM_{10}. (left) Model; (middle) observations; (right) bar plots at the individual sites from west to east. See Figure 1b for station names.

4.4. Zero-Out Emissions

[41] To explore contributions to the pollutants from local/regional sources of, for example, sulfate, OC, EC, and O_3, we reran CMAQ with complete nest-down procedures from 40.5 km to 1.5 km (Figure 1a), to obtain two additional sets of results. The first additional case was rerun without any emissions beyond D2 domain to investigate the superregional versus regional/local sources. Concentration reductions seen in this case can be attributed to the lack of superregional sources. To complement this partial emission reduction, we also ran a second set of simulations by removing emissions in PRD Economic Zone (PRDEZ) from the basic emission data (Figure 14, bottom left). This zero-

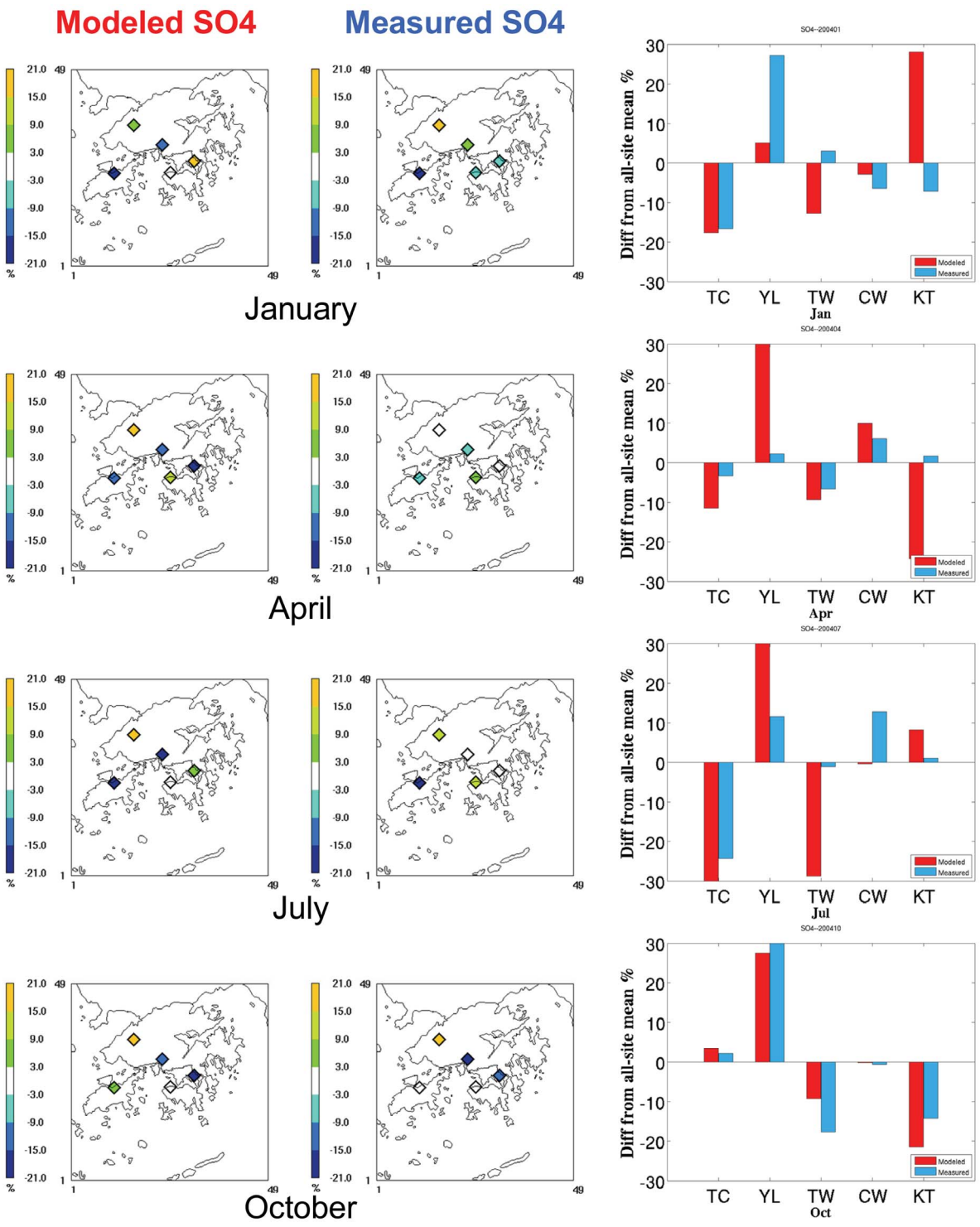

Figure 13. Percentage difference from all-site average of sulfate (EPD6DAY samples). (left) Model; (middle) observations; (right) bar plots at the individual sites from west to east. See Figure 1b for station names.

out approach was also adapted from *Streets et al.* [2007]. For convenience of discussion, the base cases are labeled BASICEMIS; the first set containing only Guangdong emissions is NOD1EMIS; and the second set without the PRDEZ emissions is NOPRDEMIS.

[42] In Figure 14, examples of spatial distributions of the complete and zeroed-out PM_{10} emissions are shown on the left; the subsequent PM_{10} concentrations three days later are displayed on the right. Differences in spatial patterns are quite obvious. However, to quantify the differences, the

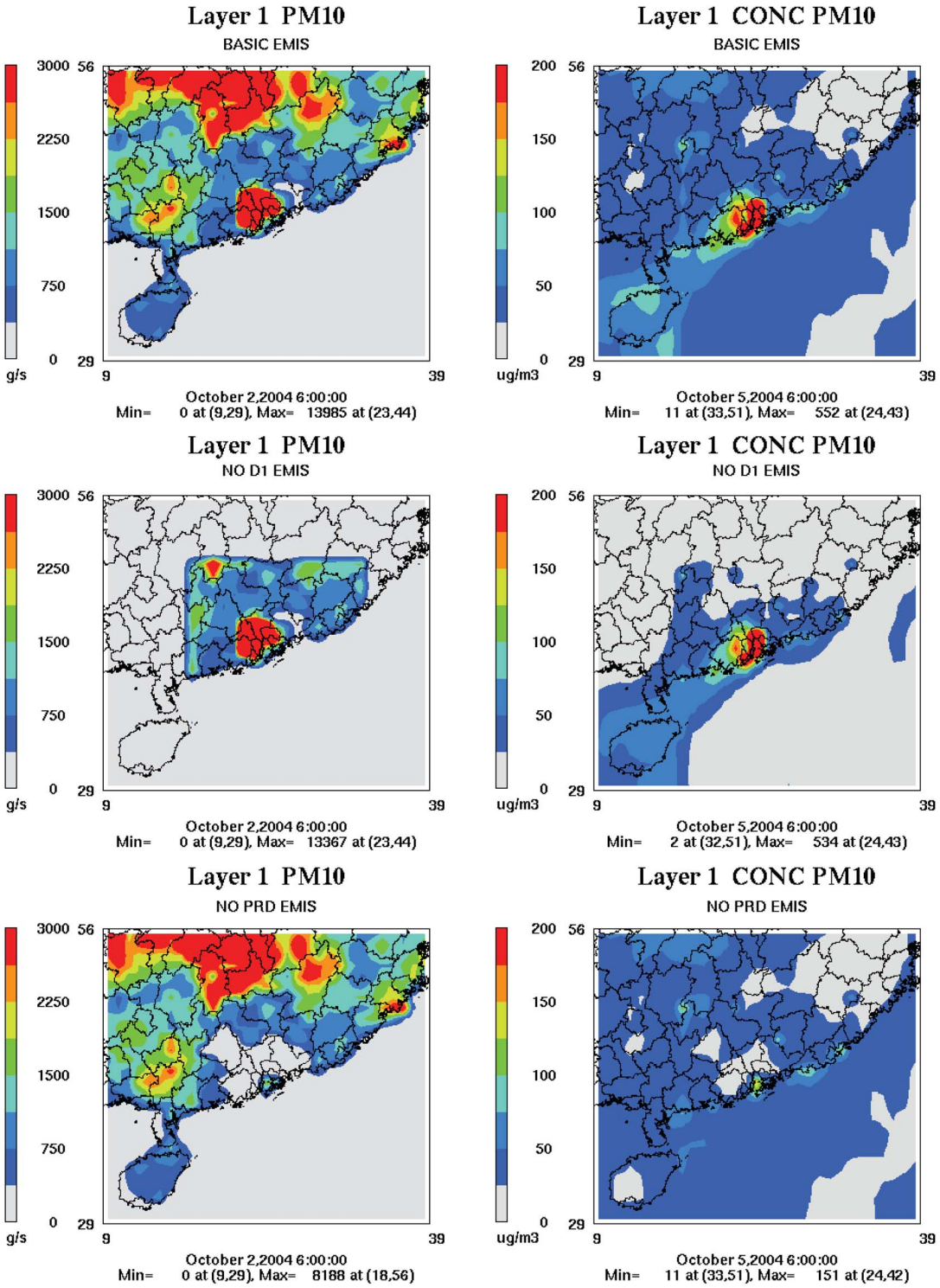

Figure 14. (left) Surface PM_{10} emissions and (right) concentrations 3 days later, in October. Top, basic; middle, Guangdong emissions retained; bottom, PRD emissions removed.

daily mean concentration level for each pollutant for each cell is averaged across the D4 (HK) domain.

[43] Thus, Figure 15 consists of bar plots of PM_{10}, $PM_{2.5}$, sulfate, OC, EC, ammonium, sea salt, and coarse/soil particles for January, April, July, and October 2004. Concentrations are averaged over a 1.5 km domain covering HK (Figure 1a). Since modeling of nitrate is less satisfactory, it is not discussed.

[44] Superregional characteristics appear in PM_{10}, $PM_{2.5}$, and $SO_4^=$ in January and October, which further supports and is consistent with measurement findings in this region [*Ho et al.*, 2003; *Cheung et al.*, 2005; *Louie et al.*, 2005b; *Wai*

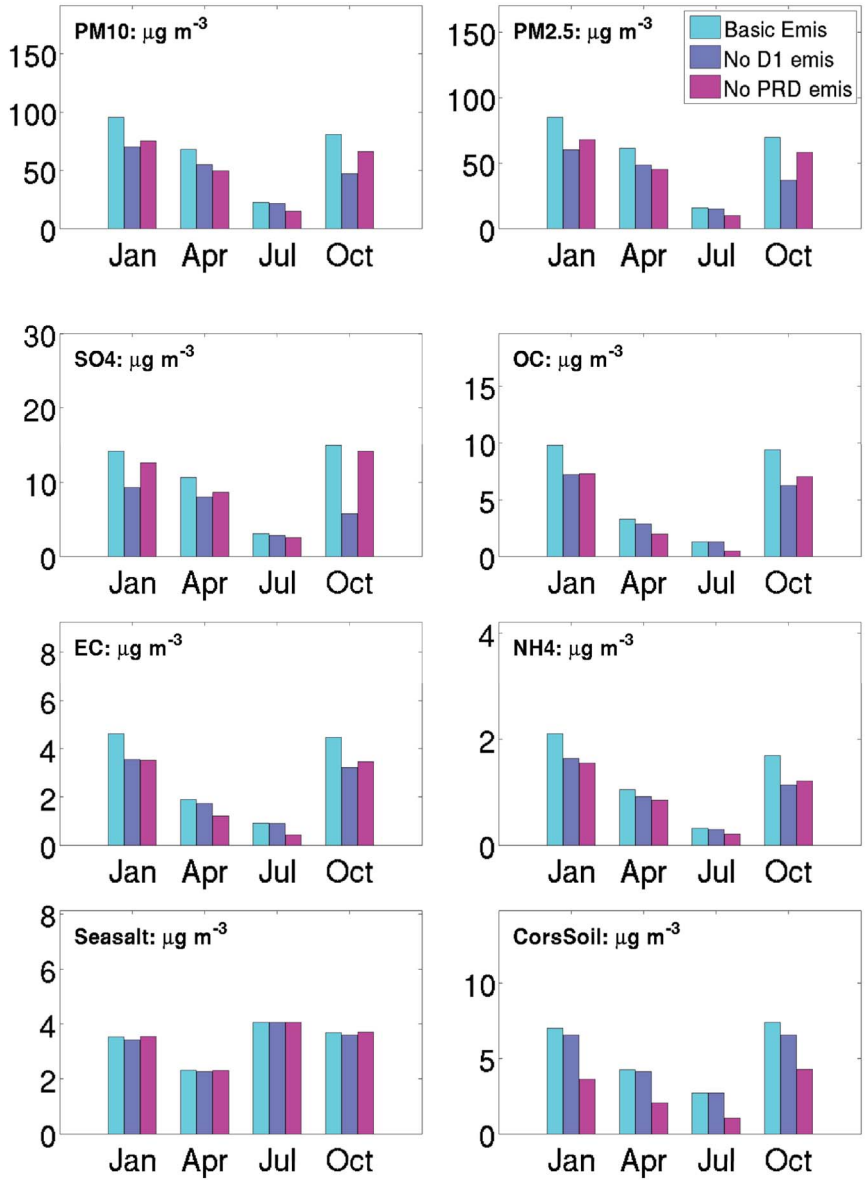

Figure 15. HK domain monthly averaged PM species in 2004. Aqua, BASICEMIS; blue, NOD1EMIS; magenta, NOPRDEMIS.

and Tanner, 2005; *So et al.*, 2007; *Guo et al.*, 2009]. Sulfate is able to travel longer distances than SO_2 owing to its longer atmospheric residence time (~4–8 days) compared to that of its precursor SO_2 (~1–4 days) [*Benkovitz et al.*, 1994; *Barth and Church*, 1999]. Ammonium, OC, and EC tend to have mixed contributions from both regional and superregional areas. For modeled chloride and sodium, there is no discernable difference across the base case and sensitivity runs, since the sea salt emission input is identical. Coarse particles and soil, on the other hand, are retained by NOD1EMIS up to ~90% of the concentrations in BASICEMIS. It is probably because the particle size range (~2.5–10 μm) is less favorable for long-distance transportation.

[45] Figure 16 displays the zero-out emission-based simulations of gaseous species SO_2, NOx, and O_3. Contrary to PM species, they exhibit much less obvious seasonal variations. In short, SO_2 is contributed both locally/regionally and superregionally. Because of relatively short lifetime compared to sulfate [*Benkovitz et al.*, 1994; *Barth and Church*, 1999], only the local/regional sources show up in the territory in April and July.

[46] NOx mainly comes from vehicles at ground level and from power plant stacks a few hundred meters above ground. Traffic patterns hardly vary from season to season, so obscure seasonality is expected. It is not surprising that NOx seems to be always locally/regionally contributed, regardless of the month of the year. The fact that NOD1EMIS level exceeds that of BASICEMIS attests to the nonlinear response of gas phase photochemistry and different paths of emission removal. This has also been demonstrated by other CMAQ

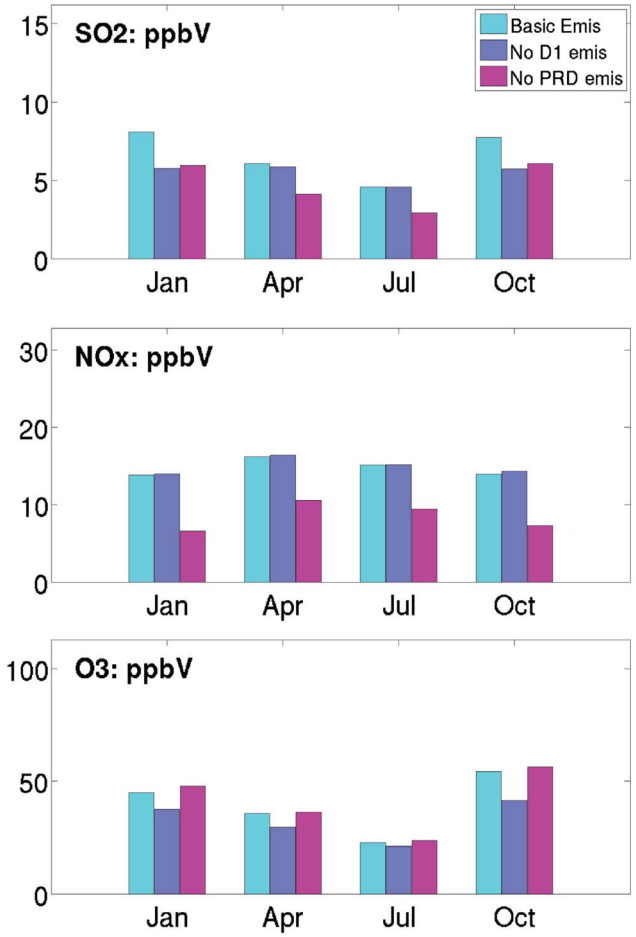

Figure 16. Same as Figure 12, except for SO_2, NOx, and O_3.

studies [*Streets et al.*, 2007]. Evidently, the bar plots suggests that O_3 is mainly transported from outside PRD, i.e., superregional areas, for January, April, and October.

[47] *Liu et al.* [1987], *Trainer et al.* [1987], *Selby* [1987], *Lin et al.* [1988], and *Sillman et al.* [1990] confirm that a reduction of either NOx or VOC emissions often increases the ozone level. The analysis becomes even more complex when NOx and VOC emissions are only removed from certain regions of the computational domains as shown in our present study. There is a sharp emission gradient between zeroed-out regions and the rest, so that emissions are redistributed spatially by the model to alter the relative proportion shared by NOx and VOC.

5. Discussion

[48] While the value of this study is hard to deny, there are certain limitations from a theoretical point of view. First of all, the zero-out approach obviously suffers from the nonlinear response of atmospheric chemistry. The suitability of such an approach depends on an intended purpose. To assess the air quality change arising from a hypothetically large-scale emission reduction, then this approach certainly has merits. But if instead the study is interested in apportioning emission sources, the subsequent results must be interpreted with care. Chemically inert species can still be accurately apportioned to their emission sources, whereas oxidized and oxidizing gases are less easily analyzed. Apart from the nonlinear response of atmospheric chemistry to partial removal of emissions, the kinetics of modeled meteorology may also be an issue. For instance, the mesoscale models MM5 and CMAQ only assume similarity theory to cater for turbulent flows, where vertical transition of horizontal wind speed is gradual. In practice, however, in urbanized areas where districts of high-rise buildings dominate, complex and discontinuous morphology dramatically alters the vertical profile of horizontal winds, giving rise to abrupt reduction in wind speeds with altitude. The current model setup does not include these features, and as a result, modeled wind speeds may be often overestimated, especially in light wind situations. In addition, mesoscale temporal and spatial resolutions might not be fine enough to resolve the turbulent transport motions often at microscales, resulting in overadvection of air and pollutant mass. Further studies into these issues will help us better understand the role of these processes.

[49] Having identified various aerosol size ranges in which substantial mass of certain PM species have gone missing, one can improve PM prediction with updated aerosol dynamics, which should include HNO_3 reactions for coarse-mode nitrate. Updated aerosol dynamics should also include speciated fine-mode sodium, chloride, potassium, and calcium, among others, for combustion sources and subsequently in fine-mode modal mass transfer.

6. Conclusions

[50] In summary, PM concentrations are higher in seasons with prevailing winds from the northeast. Sulfate, OC and EC are well reproduced by the model, compared to similar evaluations done in Europe and North America, apparently because local vehicular sources are well modeled in the emission database. Nitrate is most poorly simulated, suggesting that NOx and NH_3 emissions require further improvement. PM composition is modeled correctly for sulfate, OC, and EC. However, the portion of unidentified PM is overestimated, and constituents in the model data are unknown. Temporally, although SO_2, NOx, nitrate, and PMs are generally underestimated and O_3 overestimated, the model captures the seasonal variations in all the pollutants. In other words, the model is able to reproduce higher concentration levels in seasons with northeasterly winds and relatively lower levels under south- to southwesterly winds. The spatial gradient across HK monitoring sites is also well reproduced by the model for O_3, PM_{10}, and sulfate. Specifically, model sulfate captures all the spatial patterns in October. Modeled O_3 and PM_{10} can also match the spatial patterns in October, but less satisfactorily in July. The sulfate peaks at Yuen Long, at the rim of PRD estuary, may be due to pollutant accumulation resulting from local land-sea breeze effects. On the other hand, the O_3 troughs around central downtown sites are probably associated with their consumption by vehicle NOx. The additional zero-out sensitivity studies suggest that sulfate levels under prevailing northeasterly monsoon conditions appear to be contributed to by superregional sources, especially during October. O_3 also appears to be contributed superregionally under north-

easterly monsoon, whereas SO_2 exhibits mixed contributions from both regional and superregional areas. In view of nonlinearity in gas phase chemistry, source apportionment of emission species into individual sectors and regions seems more preferable than the zero-out approach. The Tagged Species Source Apportionment Algorithm (TSSA), for example, is one such algorithm implemented in CMAQ by *Wang et al.* [2009]. Results of this approach will be reported once this further study is accomplished.

Appendix A: Metrics for Wind Directions

[51] Compass bearings are clock arithmetic. For example, when a clockwise rotating vector at bearing 350° passed the due north by 20°, the angle made between the due north and the vector at current orientation is 10° instead of 370°, since modulus of 360° is taken. To assess the agreement in wind directions, we wish to quantify it in terms of the angular difference between observational and model winds. However, if we recklessly apply the usual IOA formula to the data, we will end up with an erroneous outcome. For instance, suppose two wind vectors are 350° and 10° to the due north. Then the vector sum is the due north. But the arithmetic average of the two numbers gives rise to 180°, i.e., due south, which is geometrically incorrect. Therefore, the IOA is modified as follows:

$$\mathrm{IOA}_{\mathrm{wdir}} = 1 - \frac{\sum_{k=1}^{N} f(|\theta_k - \phi_k|)}{180^2 N}, \quad 0^\circ \le \theta_k \le 360^\circ \text{ and } 0^\circ \le \phi_k \le 360^\circ.$$

Here,

$$f(|\theta_k - \phi_k|) = \begin{cases} |\theta_k - \phi_k|^2, & |\theta_k - \phi_k| \le 180^\circ \\ (360^\circ - |\theta_k - \phi_k|)^2, & |\theta_k - \phi_k| > 180^\circ \end{cases}$$

The restriction on the range of $|\theta_k - \phi_k|$ is based on the fact that maximal angular difference is 180°.

[52] The modified metric becomes fairly reasonable, with each pair of vectors parallel to one each other when $\mathrm{IOA}_{\mathrm{wdir}} = 1$, and in exactly opposite directions when $\mathrm{IOA}_{\mathrm{wdir}} = 0$. Between zero and unity, the $\mathrm{IOA}_{\mathrm{wdir}}$ value can indicate the extent of agreement.

[53] **Acknowledgments.** This work was supported by grants N_HKUST630/04, N_HKUST631/05SB106/07.SC06, RGC612807, RGC615406, and RTG08/09.SC001. We sincerely thank the Hong Kong Environmental Protection Department for provision of emission and air quality data and the Hong Kong Observatory for provision of meteorological data.

References

Appel, K. W., P. V. Bhave, A. B. Gilliland, G. Sawar, and S. J. Roselle (2008), Evaluation of the community multiscale air quality (CMAQ) model version 4.5: Sensitivities impacting model performance: Part II. Particulate matter. *Atmos. Environ.*, *42*, 6057–6066.

Ascher, U. M, and L. R. Petzold (1998), *Computer Methods for Ordinary Differential Equations and Differential-Algebraic Equations*, 332 pp., Society for Industrial and Applied Mathematics, Philadelphia, Pa.

Andreae, M. O., et al. (1996), Methyl halide emissions from savanna fires in southern Africa, *J. Geophys. Res.*, *101*(D19), 23,603–23,613, doi:10.1029/95JD01733.

Barth, M. C., and A. T. Church (1999), Regional and global distributions and lifetimes of sulfate aerosols from Mexico City and southeast China, *J. Geophys. Res.*, *104*(D23), 30,231–30,239, doi:10.1029/1999JD900809.

Benkovitz, C. M., R. C. Easter, S. Nemesure, R. Wagener, and S. E. Schwartz (1994), Sulfate over the North Atlantic and adjacent continental regions: Evaluation for October and November 1986 using a three-dimensional model driven by observation-derived meteorology, *J. Geophys. Res.*, *99*(D10), 20,725–20,756, doi:10.1029/94JD01634.

Bhave, P. V., S. J. Roselle, F. S. Binkowski, C. G. Nolte, S. Yu, G. L. Gipson, and K. L. Schere (2004), CMAQ aerosol module development: recent enhancements and future plans, Paper No. 6.8, CMAS Annual Conference, 18–20 Oct. 2004, Chapel Hill, NC.

Binkowski, F. S., and U. Shankar (1995), The regional particulate matter model 1. Model description and preliminary results, *J. Geophys. Res.*, *100*(D12), 26,101–26,209, doi:10.1029/95JD02093.

Binkowski, F. S. (1999), Aerosols in Models-3 CMAQ, in *Science Algorithms of the EPA Models-3 Community Multiscale Air Quality (CMAQ) Modeling System*, Rep. No. EPA/R-99/030, U.S. Environmental Protection Agency, Washington, D. C.

Binkowski, F. S., and S. J. Roselle (2003), Models-3 Community Multiscale Air Quality (CMAQ) model aerosol component 1. Model description, *J. Geophys. Res.*, *108*(D6), 4183 doi:10.1029/2001JD001409.

Byun, D. W., J. E. Pleim, R. T. Tang, and A. Bourgeois (1999a), Meteorology-chemistry interface processor (MCIP) for Models-3 Community Multiscale Air Quality (CMAQ) Modeling System, in *Science Algorithms of the EPA Models-3 Community Multiscale Air Quality (CMAQ) Modeling System*, Rep. No. EPA/600/R-99/030, U.S. Environmental Protection Agency, Washington, D. C.

Byun, D. W., J. Young, J. Pleim, M. T. Odman, and K. Alapaty (1999b), Numerical transport algorithms for the Community Multiscale Air Quality (CMAQ) chemical transport model in generalized coordinates, in *Science Algorithms of the EPA Models-3 Community Multiscale Air Quality (CMAQ) Modeling System*, Rep. No. EPA/600/R-99/030, U.S. Environmental Protection Agency, Washington, D. C.

Cao, J., S. Lee, K. Ho, S. Zou, X. Zhang, and J. Pan (2003a), Spatial and seasonal distributions of atmospheric carbonaceous aerosols in Pearl River Delta region, China, *China Particuol.*, *1*(1), 33–37.

Cao, J. J., S. C. Lee, K. F. Ho, X. Y. Zhang, S. C. Zou, K. Fung, J. C. Chow, and J. G. Watson (2003b), Characteristics of carbonaceous aerosol in Pearl River Delta region, China during 2001 winter period, *Atmos. Environ.*, *37*, 1451–1460.

Chan, C. K., and X. Yao (2008), Air pollution in mega cities in China, *Atmos. Environ.*, *42*, 1–42.

Chang, T. Y., S. J. Rudy, G. Kuntasal, and R. A. Gorse (1989), Impact of methanol vehicles on ozone air quality, *Atmos. Environ.*, *23*, 1629–1644.

Cheung, H. C., T. Wang, K. Baumann, and H. Guo (2005), Influence of regional pollution outflow on the concentrations of fine particulate matter and visibility in the coastal area of southern China, *Atmos. Environ.*, *39*, 6463–6474.

Chow, J. C., J. G. Watson, P. K. K. Louie, L. W. A. Chen, and D. Sin (2005), Comparison of $PM_{2.5}$ carbon measurement methods in Hong Kong, China, *Environ. Pollut.*, *137*, 334–344.

Duan, J., J. Tan, D. Cheng, X. Bi, W. Deng, G. Sheng, J. Fu, and M. H. Wong (2007), Sources and characteristics of carbonaceous aerosol in two largest cities in Pearl River Delta region, China, *Atmos. Environ.*, *41*, 2895–2903.

Eder, B., and S. Yu (2006), A performance evaluation of the 2004 release of Models-3 CMAQ, *Atmos. Environ.*, *40*, 4811–4824.

Fu, J. S., C. J. Jang, D. G. Streets, Z. Li, R. Kwok, R. Park, and Z. Han (2008), MICS-Asia II: Modeling gaseous pollutants and evaluating an advanced modeling system over East Asia, *Atmos. Environ.*, *42*(15), 3571–3583, doi:10.1016/j.atmosenv.2007.07.058.

Fu, J. S., D. G. Streets, C. J. Jang, J. Hao, K. He, L. Wang, and Q. Zhang (2009), Modeling regional/urban ozone and particulate matter in Beijing, China, *J. Air Waste Manage.*, *57*, 37–44.

Fang, M., M. Zheng, F. Wang, K. S. Chim, and S. C. Kot (1999), The long-range transport of aerosols from northern China to Hong Kong: A multi-technique study, *Atmos. Environ.*, *33*, 1803–1817.

Feng, Y., A. Wang, D. Wu, and X. Xu (2007), The influence of tropical cyclone Melor on PM_{10} concentrations during an aerosol episode over the Pearl River Delta region of China: Numerical modeling versus observational analysis, *Atmos. Environ.*, *41*, 4349–4365.

Gear, C. W. (1971a), *Numerical Initial Value Problems in Ordinary Differential Equations*, Prentice-Hall, Englewood Cliffs, N. J.

Gear, C. W. (1971b), The automatic integration of ordinary differential equations, *Commun. ACM*, *14*, 176–179.

Grell, G. A., J. Dudia, and D. R. Stauffer (1994), A description of the Fifth Generation Penn State/NCAR Mesoscale Model (MM5), NCAR Techni-

cal Note NCAR/TN-398+STR. (Available at http://www.mmm.ucar.edu/mm5/documents/mm5-desc-doc.html)

Guo, H., A. J. Ding, K. L. So, G. Ayoko, Y. S. Li, and W. T. Hung (2009), Receptor modeling of source apportionment of Hong Kong aerosols and the implication of urban and regional contribution, *Atmos. Environ.*, *43*(6), 1159–1169.

Hao, J., and L. Wang (2005), Improving urban air quality in China: Beijing case study, *J. Air Waste Manage. Assoc.*, *55*, 1298–1305.

He, Q., C. Li, J. Mao, A. K. H. Lau, and D. A. Chu (2008), Analysis of aerosol vertical distribution and variability in Hong Kong, *J. Geophys. Res.*, *113*, D14211, doi:10.1029/2008JD009778.

Heo, E., and Y. Feng (2005), Recent development of energy use in China at the industrial sector level. (Available at http://www.cenet.org.cn/cn/CEAC/2005in/zyhj011.doc)

Ho, K. F., S. C. Lee, J. C. Yu, S. C. Zou, and K. Fung (2002), Carbonaceous characteristics of atmospheric particulate matter in Hong Kong, *Sci. Total Environ.*, *300*, 59–67.

Ho, K. F., S. C. Lee, C. K. Chan, J. C. Yu, J. C. Chow, and X. H. Yao (2003), Characterization of chemical species in $PM_{2.5}$ and PM_{10} aerosols in Hong Kong, *Atmos. Environ.*, *37*, 31–39.

Ho, K. F., J. J. Cao, S. C. Lee, and C. K. Chan (2006), Source apportionment of $PM_{2.5}$ in urban area of Hong Kong, *J. Hazard. Mater.*, *B138*, 73–85.

Hong Kong Polytechnic University (2005), *Final Report of Determination of Suspended Particulate & VOC Emission Profiles for Vehicular Sources in Hong Kong*, Tender Ref AS 02-342.

Hong, S. Y., and H. L. Pan (1996), Nonlocal boundary layer vertical diffusion in a medium-range forecast model, *Mon. Weather Rev.*, *124*, 2322–2339.

Huang, J. P. (2005), Numerical simulation study of ozone episodes in complex terrain and coastal region, Ph.D. dissertation, Hong Kong University of Science & Technology, Hong Kong, China. (Available at http://ustlib.ust.hk/record=b909294)

Huang, J. P., J. C. H. Fung, and A. K. H. Lau (2006a), Integrated processes analysis and systematic meteorological classification of ozone episodes in Hong Kong, *J. Geophys. Res.*, *111*, D20309, doi:10.1029/2005JD007012.

Huang, X. F., J. Z. Yu, L. He, and Z. Yuan (2006b), Water-soluble organic carbon and oxalate in aerosols at a coastal urban site in China: Size distribution characteristics, sources, and formation mechanisms, *J. Geophys. Res.*, *111*, D22212, doi:10.1029/2006JD007408.

Jacobson, M. Z., and R. P. Turco (1994), SMVGEAR: A sparse-matrix, vectorized gear code for atmospheric models, *Atmos. Environ.*, *28*(2), 273–284.

Jiang, W., and H. Roth (2003), A detailed review and analysis of science, algorithms, and code in the aerosol components of Models-3/CMAQ. 1. Kinetic and thermodynamic processes in the AERO2 module, Rep. No. PET-1534-03S, Institute for Chemical Process and Environmental Technology, National Research Council of Canada, Ottawa, Canada.

Kelly, N. A., and R. F. Gunst (1990), Response of ozone to changes in hydrocarbon and nitrogen oxide concentrations in outdoor smog chambers with Los Angeles air, *Atmos. Environ.*, *24A*, 2991–3005.

Khan, A. A., W. de Jong, P. J. Jansens, and H. Spliethoff (2009), Biomass combustion in fluidized bed boilers: Potential problems and remedies, *Fuel Proc. Tech.*, *90*, 21–50.

Kim Oanh, N. T., et al. (2006), Particulate air pollution in six Asian cities: Spatial and temporal distributions, and associated sources, *Atmos. Environ.*, *40*, 3367–3380.

Lin, X., M. Trainer, and S. C. Liu (1988), On the nonlinearity of tropospheric ozone production, *J. Geophys. Res.*, *93*(D12), 15,879–15,888, doi:10.1029/JD093iD12p15879.

Liu, S. C., M. Trainer, F. C. Fehsenfeld, D. D. Parrish, E. J. Williams, D. W. Fahey, G. Hübler, and P. C. Murphy (1987), Ozone production in the rural troposphere and implications for regional and global ozone distributions, *J. Geophys. Res.*, *92*(D4), 4191–4207, doi:10.1029/JD092iD04p04191.

Lo, J. C. F., A. K. H. Lau, J. C. H. Fung, and F. Chen (2006), Investigation of enhanced cross-city transport and trapping of air pollutants by coastal and urban land-sea breeze circulations, *J. Geophys. Res.*, *111*, D14104, doi:10.1029/2005JD006837.

Lo, J. C. F., A. K. H. Lau, F. Chen, J. C. H. Fung, and K. K. M. Leung (2007), Urban modification in a mesoscale model and the effects on the local circulation in the Pearl River Delta region, *J. Appl. Meteorol. Climat.*, *46*, 457–476.

Louie, P. K. K., J. C. Chow, L. W. A. Chen, J. G. Watson, G. Leung, and D. W. M. Sin (2005a), $PM_{2.5}$ chemical composition in Hong Kong: Urban and regional variations, *Sci. Total Environ.*, *338*, 267–281.

Louie, P. K. K., J. G. Watson, J. C. Chow, A. Chen, D. W. M. Sin, and A. K. H. Lau (2005b), Seasonal characteristics and regional transport of $PM_{2.5}$ in Hong Kong, *Atmos. Environ.*, *39*, 1695–1710.

Lu, R., R. P. Turco, and M. Z. Jacobson (1997), An integrated pollution modeling system for urban and regional scales: 2. Simulations for SCAQS 1987, *J. Geophys. Res.*, *102*(D5), 6081–6098, doi:10.1029/96JD03502.

Malwer, E. J., S. J. Taubman, P. D. Brown, M. J. Iacono, and S. A. Clough (1997), Radiative transfer for inhomogeneous atmosphere: PRTM, validated correlated-k model for the longwave, *J. Geophys. Res.*, *102*(D14), 16,663–16,682.

McCulloch, A., M. L. Aucott, C. M. Benkovitz, T. E. Graedel, G. Kleiman, P. M. Midgley, and Y.-F. Li (1999), Global emissions of hydrogen chloride and chloromethane from coal combustion, incineration and industrial activities: reactive chlorine emissions inventory, *J. Geophys. Res.*, *104*(D7), 8391–8403, doi:10.1029/1999JD900025.

Pleim, J. E., and J. S. Chang (1992), A non-local closure model for vertical mixing in the convective boundary layer, *Atmos. Environ.*, *26A*, 965–981.

Reff, A., P. V. Bhave, H. Simon, T. G. Pace, G. A. Pouliot, J. D. Mobley, and M. Houyoux (2009), Emissions inventory of $PM_{2.5}$ trace elements across the United States, *Environ. Sci. Technol.*, *43*, 5790–5796.

Reid, R. C., J. M. Prausnitz, and B. E. Poling (1987), *The Properties of Gases and Liquids*, 4th ed., pp. 587–588, McGraw-Hill, New York.

Seinfeld, J. H., and S. N. Pandis (1998), *Atmospheric Chemistry and Physics: From Air Pollution to Climate Change*, Wiley, New York.

Selby, K. (1987), A modeling study of atmospheric transport and photochemistry in the mixed layer during anticyclonic episodes in Europe, II, Calculations of photo-oxidant levels along air trajectories, *J. Clim. Appl. Meteorol.*, *26*, 1317–1338.

Sillman, S., J. A. Logan, and S. C. Wofsy (1990), The sensitivity of ozone to nitrogen oxides and hydrocarbons in regional ozone episodes, *J. Geophys. Res.*, *95*(D2), 1837–1851, doi:10.1029/JD095iD02p01837.

Simpson, D., K. E. Yttri, Z. Klimont, K. Kupiainen, A. Caseiro, A. Gelencser, C. Pio, H. Puxbaum, and M. Legrand (2007), Modeling carbonaceous aerosol over Europe: Analysis of the CARBOSOL and EMEP EC/OC campaigns, *J. Geophys. Res.*, *112*, D23S14, doi:10.1029/2006JD008158.

So, K. L., H. Guo, and Y. S. Li (2007), Long-term variation of $PM_{2.5}$ levels and composition at rural, urban, and roadside sites in Hong Kong: Increasing impact of regional air pollution, *Atmos. Environ.*, *41*, 9427–9434.

Streets, D. G., et al. (2003), An inventory of gaseous and primary aerosol emissions in Asia in the year 2000, *J. Geophys. Res.*, *108*(D21), 8809, doi:10.1029/2002JD003093.

Streets, D. G., C. Yu, M. H. Bergin, X. Wang, and G. R. Carmichael (2006), Modeling study of air pollution due to the manufacture of export goods in China's Pearl River Delta, *Environ. Sci. Technol.*, *40*(7), 2099–2107, doi:10.1021/es051275n.

Streets, D. G., et al. (2007), Air quality during the 2008 Beijing Olympic Games, *Atmos. Environ.*, *41*(3), 480–492.

Trainer, M., E. J. Williams, D. D. Parrish, M. P. Buhr, E. J. Allwine, H. H. Westberg, F. G. Fehsenfeld, and S. C. Liu (1987), Models and observations of the impact of natural hydrocarbons on rural ozone, *Nature*, *329*, 705–707.

Tsang, H., R. Kwok, and A. H. Miguel (2008), Pedestrian exposure to ultrafine particles in Hong Kong under heavy traffic conditions, *Aerosol Air Qual. Res.*, *8*(1), 19–27.

U.S. Environmental Protection Agency (1991), Guidance for Regulatory Application of the Urban Airshed Model (UAM), Office of Air Quality Planning and Standards, U.S. Environmental Protection Agency, Research Triangle Park, N. C.

U.S. Environmental Protection Agency (2000), SPECIATE data base V.3. 1, Washington, D. C.

Wai, K. M., and P. Tanner (2005), Relationship between ionic composition in PM_{10} and the synoptic-scale and mesoscale weather conditions in a south China coastal city: A 4-year study, *J. Geophys. Res.*, *110*, D18210, doi:10.1029/2004JD005385.

Wang, T. (2003), Study of visibility reduction and its causes in Hong Kong, Tender Ref. AS 01-286, Final Report for Air Services Group, Hong Kong Environmental Protection Department.

Wang, Z. S., C.-J. Chien, and G. S. Tonnesen (2009), Development of a tagged species source apportionment algorithm to characterize three-dimensional transport and transformation of precursors and secondary pollutants, *J. Geophys. Res.*, *114*, D21206, doi:10.1029/2008JD010846.

Wei, X. L., Y. S. Li, K. S. Lam, A. Y. Wang, and T. J. Wang (2007), Impact of biogenic VOC emissions on a tropical cyclone-related ozone episode in the Pearl River Delta region, China, *Atmos. Environ.*, *41*, 7851–7864.

Wu, W. M. (2003), Statistical analysis on SO_2, O_3, and PM_{10} in Hong Kong, Master's thesis, Department of Mathematics, Hong Kong University of Science & Technology, Hong Kong, China.

Wu, Y., J. Hao, L. Fu, J. Hu, Z. Wang, and U. Tang (2003), Chemical characteristics of airborne particulate matter near major roads and at background locations in Macao, China, *Sci. Total Environ.*, *317*, 195–172.

Yu, J. Z., J. W.T. Tung, A. W. M. Wu, A. K. H. Lau, P. K. K. Louie, and J. C. H. Fung (2004), Abundance and seasonal characteristics of elemental and organic carbon in Hong Kong PM_{10}, *Atmos. Environ.*, *38*, 1151–1521.

Yuan, Z., A. K. H. Lau, H. Zhang, J. Yu, P. K. K. Louie, and J. C. H. Fung (2006), Identification and spatiotemporal variations of dominant PM_{10} sources over Hong Kong, *Atmos. Environ.*, *40*(10), 1803–1815, doi:10.1016/j.atmosenv.2005.11.030.

Zheng, M., G. S. W. Hagler, L. Ke, M. H. Bergin, F. Wang, P. K. K. Louie, L. Salmon, D. W. M. Sin, J. Z. Yu, and J. Schauer (2006), Composition and sources of carbonaceous aerosols at three contrasting sites in Hong Kong, *J. Geophys. Res.*, *111*, D20313, doi:10.1029/2006JD007074.

J. S. Fu, Department of Civil & Environmental Engineering, University of Tennessee, 8803 Simpson Road, Knoxville, TN 37920, USA.

J. C. H. Fung and R. H. F. Kwok, Department of Mathematics, Hong Kong University of Science and Technology, Clear Water Bay, Kowloon, Hong Kong. (rkwokhf@ust.hk)

A. K. H. Lau, Division of Environment, Hong Kong University of Science and Technology, Clear Water Bay, Kowloon, Hong Kong.